

Nucleation of rupture under slip dependent friction law: simple models of fault zone

J.-P. Ampuero and J.-P. Vilotte

Département de Sismologie, Institut de Physique du Globe de Paris, Paris, France

F.J. Sánchez-Sesma

Instituto de Ingeniería, UNAM, México D.F., México

Abstract. The initiation of frictional instability is investigated for simple models of fault zone using a linearized perturbation analysis. The fault interface is assumed to obey a linear slip weakening law. The fault is initially pre-stressed uniformly at the sliding threshold. In the case of anti-plane shear between two homogeneous linearly elastic media, space-time and spectral solutions are obtained and shown to be consistent. The nucleation is characterized by: (1) a long wavelength unstable spectrum bounded by a critical wavenumber; (2) an exponential growth of the unstable modes; and (3) an induced off-fault deformation that remains trapped within a bounded zone in the vicinity of the fault. These phenomena are characterized in terms of the elastic parameters of the surrounding medium and a nucleation length that results from the coupling between the frictional interface and the bulk elasticity. These results are extended to other geometries within the same formalism and implications for 3D rupture are discussed. Finally, internal fault structures are investigated in terms of a fault-parallel damaged zone. Spectral solutions are obtained for both a smooth and a layered distribution of damage. For natural faults the nucleation is shown to depend strongly on the existence of an internal damaged layer. This nucleation can be described in terms of an effective homogeneous model. In all cases, frictional trapping of the deformation out of the fault can lead to the property that arbitrarily long wavelengths remain sensitive to the existence of a fault zone.

1. Introduction

Earthquake source nucleation is a key intrinsic part of the dynamic earthquake rupture. Its understanding is crucial for modern source mechanics studies and may attract interest as an immediate earthquake precursor. The existence of a nucleation phase preceding unstable dynamic rupture propagation has long been recognized in high resolution large-scale experiments on frictional slip propagation along a pre-cut fault [Dieterich, 1978; Dieterich *et al.*, 1978; Dieterich, 1981; Okubo and Dieterich, 1984; Ohnaka and Yamamoto, 1984; Ohnaka *et al.*, 1987a, b]. Ohnaka and coworkers have shown that unstable frictional slip propagation is preceded by an initial nucleus of micro-slip instabilities localized within a zone of limited size compared to that of the rock sample. The nucleation process itself is characterized by a slow and stable growth of the slipping nucleus followed by an unstable accelerating phase which eventually leads to an inertial rupture [Ohnaka, 1986; Ohnaka *et al.*, 1987a, b; Ohnaka and Yamashita, 1989; Yamashita and Ohnaka, 1991; Ohnaka, 1996]. The nucleation process has been shown to depend on properties of the pre-cut fault surfaces like the roughness [Ohnaka and Shen, 1999].

In detailed seismological observations [Iio, 1992, 1995; Ellsworth and Beroza, 1995; Beroza and Ellsworth, 1996; Ellsworth and Beroza, 1998; Iio *et al.*, 1999] precursory phases associated to some stage of the earthquake nucleation process have

been recorded, even though the shape of this initial signal is not universal [Ishira *et al.*, 1992; Fukao and Shibasaki, 1995; Mori and Kanamori, 1996]. Moreover, the underlying slipping process which is believed to occur within the earthquake nucleation zone may trigger clustered foreshocks over a zone of limited extension [Dodge *et al.*, 1995, 1996].

Recently, mathematical and numerical models, based on slip-weakening or rate-and-state friction laws, have been developed to investigate the initiation process (i.e. the transition between a stable quasi-static rupture growth to an unstable high-speed rupture propagation) associated with a progressive weakening of shear strength within a localized nucleation zone [Yamashita and Ohnaka, 1991; Matsu'ura *et al.*, 1992; Dieterich, 1992; Dieterich and Kilgore, 1996; Kato and Hirasawa, 1997; Shibasaki and Matsu'ura, 1998; Sato and Kanamori, 1999; Lapusta *et al.*, 2000]. An interesting model by Campillo and Ionescu [1997] provides a spectral analysis of the linear stability problem associated to the initiation of anti-plane shear instability under slip weakening friction in a fault prestressed up to its frictional threshold. Even though this analysis is restricted to a simplistic initial state of the fault, it provides valuable insights on the dynamics of the nucleation. In particular, these authors proposed a scaling of the duration of the nucleation and of the shortest unstable length scale upon the frictional weakening rate [Campillo and Ionescu, 1997; Ionescu and Campillo, 1999]. Such an analysis was further extended to more general geometry [Favreau *et al.*, 1999, 2000; Favreau, 2000] and finite fault segments [Dascalescu *et al.*, 2000; Voisin *et al.*, 2000]. However, some questions on the validity of this analysis were recently raised by Knopoff *et al.* [2000] who also proposed a new method based upon a boundary integral formulation of the associated anti-plane problem.

Copyright 2001 by the American Geophysical Union.

Paper number 2001JB000452.
0148-0227/02/2001JB000452\$9.00

To date, most of these models have considered only simplified problems in which the fault is a contact plane within a uniform elastic medium. Structurally, major faults are generally embedded in a fault-parallel damaged zone with a width of few hundred meters to a few kilometers. Evidence for internal structure of faults has come from exhumed faults [Wallace and Morris, 1986; Chester et al., 1993], surface expression of active faults [Sieh et al., 1993], borehole data [Ito et al., 1999] and seismic profiling and tomography [Michelini and McEvilly, 1991; Scott et al., 1994; Thurber et al., 1997]. The fault zone is the result of previous rupture history and is often characterized by a centralized layer of highly comminuted gouge bounded by a much thicker zone of damaged host rock. The structure of the fault zone has been recently investigated with the aid of fault-zone trapped waves arising from coherent multiple reflections at the boundary between the damaged zone and the surrounding rock [Ben-Zion and Aki, 1990; Li and Leary, 1990; Li and Vidale, 1996; Ben-Zion, 1998; Li et al., 1999]. The internal structure of faults is still not well understood but may introduce additional length scales into the rupture process and be of great importance for understanding how earthquakes come about. Recently, it has been shown that such damaged fault zone may have a significant effect on rupture dynamics [Harris and Day, 1997; Andrews and Ben-Zion, 1997; Cochard and Rice, 2000]. Such fault structure may play an important role during the nucleation process of an earthquake.

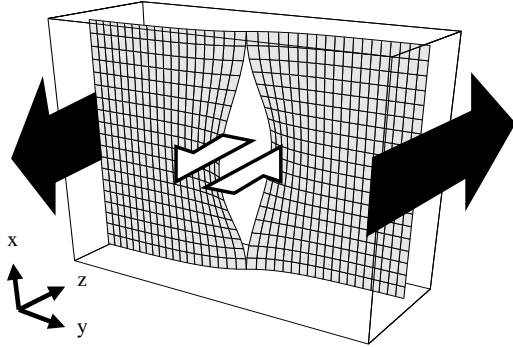


Figure 1. A homogeneous and infinite linearly elastic medium subjected to anti-plane shearing. The assumed translational invariance along the z axis makes the problem 2D. The displacement is parallel to the z direction. The gray surface is the displacement of an iso- z slice as induced by an external shear load (black arrows). Non uniform slip (displacement discontinuity indicated by white arrows) can take place on a pre-existent fault plane Γ at $y = 0$.

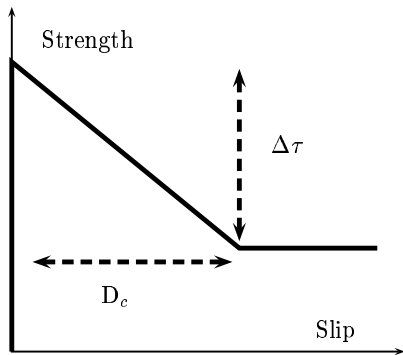


Figure 2. Linear slip-weakening interface law: the tangential shear strength is plotted against the tangential slip on the fault interface. When the yield strength τ_s is reached, slip can occur and the shear strength drops linearly to a dynamic value τ_d . The characteristic distance D_c over which the stress drop $\Delta\tau = \tau_s - \tau_d$ takes place, is related to the surface energy.

In this study, we investigate the initiation of frictional slip instability of an anti-plane shear fault under slip-dependent friction. In spite of its simplicity this problem retains the basic ingredients that are believed to be of importance during the nucleation process. Formulated as a generalized Lamb's problem it can be regarded as a basic physical model of importance in the fields of wave propagation, contact mechanics and seismic source. We first consider anti-plane shearing of two homogeneous linearly elastic half-spaces in contact. Time domain and spectral solutions are independently derived and shown to be consistent. Based on these solutions, the dynamics of slip and deformation within the bulk are explicitly characterized. A general spectral framework is proposed to extend these results to other geometries and implications for 3D rupture nucleation are discussed. We then extend the analysis to more realistic fault zones. In particular, we investigate the influence of a fault-parallel damaged zone on the nucleation and its potential implication in terms of the effective behavior of the interface.

2. Anti-plane shear in a homogeneous elastic space

Interest is focused first on anti-plane shearing of two homogeneous linearly elastic half-spaces. Figure 1. The elastic media are characterized by a shear modulus μ , a mass density ρ and therefore a shear wave velocity $\beta = \sqrt{\mu/\rho}$. With respect to a Cartesian reference frame, $(\hat{x}, \hat{y}, \hat{z})$, the contact plane Γ is defined by $y = 0$. Translational invariance is assumed along \hat{z} , making the problem 2D. The displacement is polarized along \hat{z} , $\mathbf{u} = w(x, y, t) \hat{z}$. The non null stress components are $\sigma_{zx} = \sigma_{zx}^0 + \mu \partial_x w(x, y, t)$, $\sigma_{zy} = \sigma_{zy}^0 + \mu \partial_y w(x, y, t)$ and $\sigma_{yy} = \sigma_{yy}^0$, where σ^0 is the initial stress. Slip is defined as the displacement discontinuity across Γ , $D(x, t) \doteq w(x, 0^+, t) - w(x, 0^-, t)$. In both elastic media the displacement field $w(x, y, t)$ is governed by a scalar wave equation. Taking into account the symmetry, $w(x, y, t) = -w(x, -y, t)$, the problem can be restricted to the half-space $y \geq 0$.

The interactions between two elastic media are generally dealt by specifying an interface law. A large amount of work has been done, in the last decades, using rate and state friction laws [Scholz, 1998; Marone, 1998]. Ohnaka and co-workers [Ohnaka et al., 1987b; Ohnaka and Shen, 1999] measured experimentally a slip weakening of the shear strength as a first order effect during the nucleation process. A linear slip weakening law [Andrews, 1976] is considered here, see Figure 2. In both friction laws, one of the main ingredient is the existence of an internal length, a feature that we believe to control generic properties of the nucleation process. However this will require further scrutiny. For the slip weakening friction law, slip occurs when traction reaches a yield strength τ_s . As slip evolves, the shear strength decreases linearly down to a residual value, the dynamic strength τ_d . Full strength drop, $\Delta\tau = \tau_s - \tau_d$, is reached for a characteristic slip D_c , an interface length that can be related to surface energy. Without an explicit loading/unloading criterion, the interface law is more related to a surface potential than to a friction law besides local monotonic loading. In the remaining, the material properties will be assumed uniform along the fault.

The interface law is intrinsically non regular, due to the existence of a strength threshold. A regular problem is however obtained when the fault is initially at the onset of sliding, i.e. when initial traction equals the yield strength. Even though such an initial state is more a mathematical ersatz than a realistic physical condition, it allows to study analytically the motion induced by a traction perturbation $T_0(x, t)$. Such analytical solutions do provide valuable insights on the physics of the nucleation process. As long as

the characteristic slip D_c has not been reached somewhere on the fault, the response to a perturbation is governed by the following linear problem

$$\frac{\partial^2 w}{\partial x^2} + \frac{\partial^2 w}{\partial y^2} = \frac{1}{\beta^2} \frac{\partial^2 w}{\partial t^2} \quad \text{for } y > 0 \quad (1)$$

$$-\mu \frac{\partial w}{\partial y} = T_0(x, t) + 2\gamma w \quad \text{for } y = 0 \quad (2)$$

with initial conditions $w(x, y, 0) = 0$ and $\frac{\partial w}{\partial t}(x, y, 0) = 0$. The slip weakening rate of the contact interface is defined as:

$$\gamma \doteq \frac{\Delta\tau}{D_c} \quad (3)$$

The basic length scale of this problem, α^{-1} , arises from the competition between bulk elasticity and slip weakening rate:

$$\alpha \doteq 2\gamma/\mu \quad (4)$$

2.1. A time domain solution

Let consider the response to an impulse load $T_0(x, t) = T_0 \delta(x) \delta(t)$, where T_0 has the dimension of force \times time. This elementary solution is to be understood as the Green's function of the linear problem. The response to more general loading, or more general initial conditions like in [Campillo and Ionescu, 1997], can be obtained from it by standard numerical convolution.

In order to solve the problem, let first introduce a virtual deformation field $\Psi(x, y, t)$ implicitly defined, as in [Campillo and Ionescu, 1997], by:

$$\frac{\partial \Psi}{\partial y} = \alpha w + \frac{\partial w}{\partial y} \quad (5)$$

The original problem for w is equivalent to Lamb's problem for Ψ :

$$\frac{1}{\beta^2} \frac{\partial^2 \Psi}{\partial t^2} = \frac{\partial^2 \Psi}{\partial x^2} + \frac{\partial^2 \Psi}{\partial y^2} \quad \text{for } y > 0 \quad (6)$$

$$-\mu \frac{\partial \Psi}{\partial y} = T_0 \delta(x) \delta(t) \quad \text{along } y = 0 \quad (7)$$

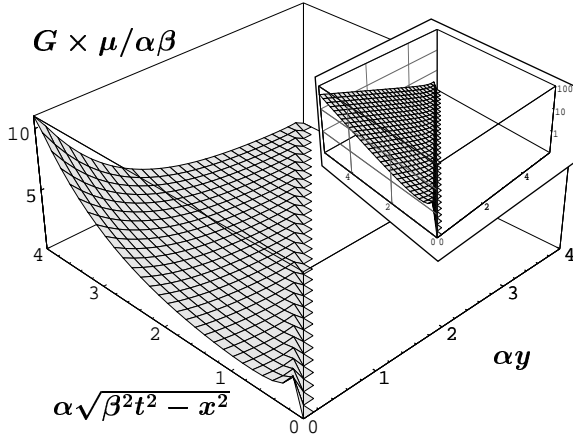


Figure 3. Green's function for the anti-plane shearing along a slip weakening interface within an homogeneous linearly elastic medium. The Green's function is plotted as a function of αy , the normalized distance off the fault, and $\alpha \sqrt{\beta^2 t^2 - x^2}$. The inset shows a log-plot. Behind the front pulse, the displacement exhibits an exponential decay out of the fault and an exponential growth with time.

with initial conditions $\Psi(x, y, 0) = 0$ and $\frac{\partial \Psi}{\partial t}(x, y, 0) = 0$. Its solution is

$$\Psi(x, y, t) = \frac{T_0 H(t - r/\beta)}{\mu\pi \sqrt{t^2 - r^2/\beta^2}} \quad (8)$$

where H is the Heaviside step function and $r^2 = x^2 + y^2$. The displacement is found solving (5) with (8), see Appendix A, using a Laplace transform with respect to y , taking carefully into account the boundary condition at $y = 0$. A useful representation of the displacement field in terms of the Lamb's solution is obtained:

$$w(x, y, t) = \Psi(x, y, t) + \alpha e^{-\alpha y} \int_y^\infty \Psi(x, \zeta, t) e^{\alpha \zeta} d\zeta \quad (9)$$

Owing to the causality of Ψ , the second term in (9) need to be integrated only within the causality cone, i.e. from y to $Y(x, t) \doteq \sqrt{\beta^2 t^2 - x^2}$ when $r \leq \beta t$. As a result, the solution of the slip weakening problem also obeys to the causality principle. Moreover, the motion depends on (x, t) only through $\sqrt{\beta^2 t^2 - x^2}$.

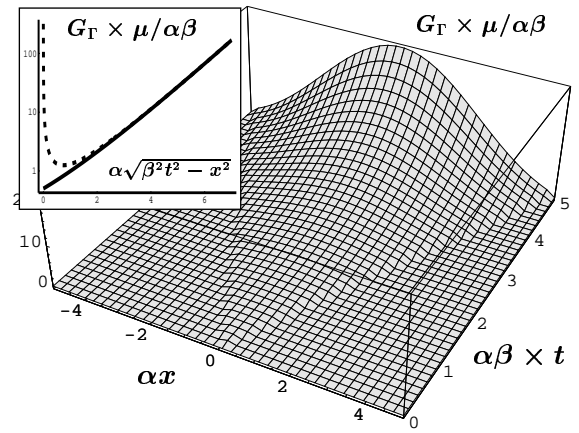


Figure 4. The interface Green's function $G_\Gamma(x, t)$. The front pulse has been removed here for clarity. The Gaussian shape is related to an underlying diffusion process. The inset shows a log-plot as a function of $\sqrt{\beta^2 t^2 - x^2}$. The complete solution, with the Lamb's pulse, is shown there by a dashed line. The main feature is an exponential growth with time.

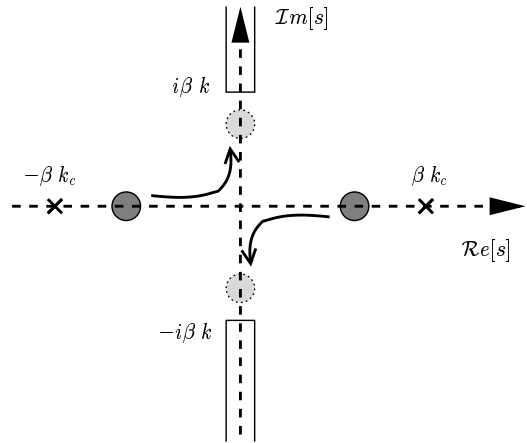


Figure 5. Poles (filled circles) and branch cuts (boxed axis) of the interface Green's function for anti-plane shear in homogeneous medium. The evolution of the poles as $|k|$ increases is shown by arrows.

When the fault can slip freely, i.e. $\alpha = 0$, this second term vanishes and the Lamb's solution is recovered. In the case of slip weakening, $\alpha > 0$, the displacement left on the wake of the Lamb's pulse, where $|y| \ll Y(x, t)$, decays exponentially as a function of the distance to the fault. The characteristic depth of penetration of the induced bulk deformation is α^{-1} , see Figure 3.

Furthermore a compact analytical expression for the slip can be worked out. From (8) and (9)

$$D(x, t) = 2 \frac{T_0}{\mu} H(\beta t - |x|) \left\{ \frac{1}{\pi \sqrt{t^2 - x^2/\beta^2}} + \alpha \int_0^{Y(x, t)} \frac{e^{\alpha \zeta} d\zeta}{\pi \sqrt{t^2 - (x^2 + \zeta^2)/\beta^2}} \right\} \quad (10)$$

The last integral can be expressed in terms of the modified Bessel and Struve functions making use of the relation [Gradshteyn and Ryzhik, 1965, eq. 3.387.5]

$$\int_0^1 \frac{e^{z\eta}}{\pi \sqrt{1-\eta^2}} d\eta = \frac{1}{2} \{L_0 + I_0\}(z) \quad (11)$$

Finally, the slip evolution, Figure 4, is given by

$$D(x, t) = 2 \frac{T_0}{\mu} H(\beta t - |x|) \left[\frac{1}{\pi \sqrt{t^2 - x^2/\beta^2}} + \frac{\alpha \beta}{2} \{L_0 + I_0\} \left(\alpha \sqrt{\beta^2 t^2 - x^2} \right) \right] \quad (12)$$

In contrast to the solution of [Campillo and Ionescu, 1997], this provides an explicit solution in the space and time domain which is found to agree with the original solution by Knopoff et al. using a boundary integral procedure [Knopoff et al., 2000, eq. 16].

2.2. A Spectral solution

Deeper understanding can be obtained by a spectral domain inspection. Using Fourier transform in x and one-sided Laplace transform in t , with the corresponding transformed variables k and s , the displacement is independently shown to be, see Appendix B,

$$w(k, y, s) = G(k, y, s) \times T_0(k, s) \quad (13)$$

$$G(k, y, s) = \frac{e^{-\nu y}}{\mu(\nu - \alpha)} \quad (14)$$

where $\nu(k, s) \doteq \sqrt{k^2 + s^2/\beta^2}$ is defined to have a positive real part in order to respect radiation conditions out from the fault. Such a spectral approach has been shown in previous studies of [Campillo and Ionescu, 1997] et coworkers to be consistent with direct numerical simulations based on finite difference methods. Moreover, the spectral Green function $G(k, y, s)$ can be transformed back to the (x, y, t) domain to check its consistency with the result of the previous section, see Appendix B.

In the following, the interest is focused on the response on the fault itself. The interface Green function G_Γ , that relates the slip response $D(k, s)$ along the interface to a loading perturbation $T_0(k, s)$ is defined by

$$G_\Gamma(k, s) \doteq 2 G(k, y=0, s) = \frac{2/\mu}{\nu - \alpha} \quad (15)$$

In the complex s plane, G_Γ has poles and branch cuts singularities. Their respective contribution can be isolated using a residue technique

$$G_\Gamma(k, s) = \frac{2/\mu}{\nu + \alpha} + \frac{4\alpha/\mu}{\nu^2 - \alpha^2} \doteq G_b(k, s) + G_p(k, s) \quad (16)$$

The branch cuts contribution is denoted here as G_b and clearly the branch cuts of G_Γ are those of ν . As shown in Figure 5, they emanate from $\pm i\beta|k|$ and move to $\pm i\infty$. As they lie on the imaginary axis, they only involve stable and purely propagative (real frequency) modes: the branch cuts do not contribute to the long term behavior. Noting that G_b is identical to G_Γ when α is replaced by $-\alpha$, the branch cuts contribution is analogous to a slip strengthening process and therefore is not expected to have an unstable behavior. The back transform of G_b to the (x, t) domain is obtained by changing α to $-\alpha$ in (12) and making use of the symmetry properties of I_0 and L_0 :

$$G_b(x, t) = \frac{2}{\mu} H(\beta t - |x|) \left[\frac{1}{\pi \sqrt{\beta^2 t^2 - x^2}} + \frac{\alpha \beta}{2} \{L_0 - I_0\} \left(\alpha \sqrt{\beta^2 t^2 - x^2} \right) \right] \quad (17)$$

Asymptotically, L_0 and I_0 cancel each other and the branch cut contribution vanishes for $t \gg x/\beta$ as $O(1/t)$.

G_p in (16) stands for the contribution of the poles. It can be transformed back in the (x, t) domain, see Appendix B,

$$G_p(x, t) = \frac{2}{\mu} H(\beta t - |x|) \alpha \beta I_0 \left(\alpha \sqrt{\beta^2 t^2 - x^2} \right) \quad (18)$$

For $t \gg x/\beta$, this expression diverges as $e^{\alpha \beta t}/\sqrt{\alpha \beta t}$. However, not all the wavelengths have an unstable contribution. Indeed, the expression of G_p in the (k, t) domain is:

$$G_p(k, t) = 2\alpha\beta \frac{\sinh(\beta\sqrt{\alpha^2 - k^2}t)}{\sqrt{\alpha^2 - k^2}} \quad \text{if } |k| \leq \alpha \quad (19)$$

$$= 2\alpha\beta \frac{\sin(\beta\sqrt{k^2 - \alpha^2}t)}{\sqrt{k^2 - \alpha^2}} \quad \text{if } |k| \geq \alpha$$

This defines a critical wavenumber

$$k_c = \alpha \quad (20)$$

Only the long wavelengths of a perturbation, $|k| < k_c$, diverge exponentially and trigger an instability. For each wavenumber, there

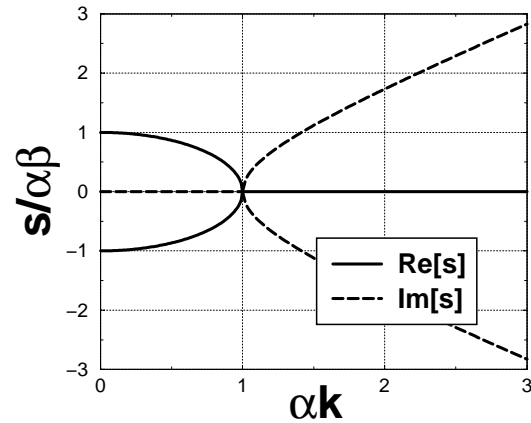


Figure 6. Real and imaginary parts of the poles of the homogeneous anti-plane shear problem as a function of wavenumber. The elliptic branch, corresponding to subcritical wavenumbers $|k| < k_c$, has an unstable branch (in the upper plane $Re[s] > 0$). The hyperbolic branch for supercritical wavenumbers corresponds to propagative modes.

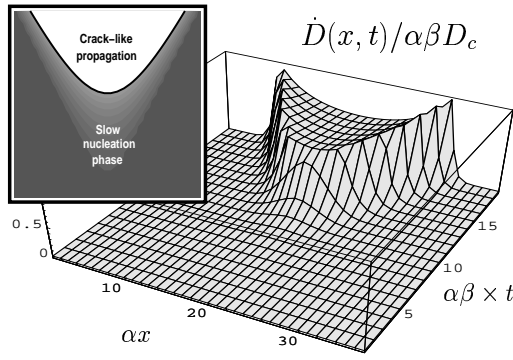


Figure 7. Typical slip rate and slip (contours in the inset) after a perturbation at $x = 20/\alpha$, as resulting from a numerical simulation using the BIEM formulation of *Cochar and Madariaga* [1996]. The onset of the crack-like propagation is delayed by the slow nucleation phase. The rupture front is hyperbolic and initially supershear but remains inside the causality cone of the triggering perturbation.

are two poles

$$s_{\pm}(k) = \pm\beta\sqrt{k_c^2 - k^2} \quad (21)$$

As shown in Figure 5 they emanate from $\pm\beta k_c$ for $k = 0$, then move along the real axis, collapse at the origin for $|k| = k_c$ and finally switch to the imaginary axis where they tend toward $\pm i\beta|k|$. Their real and imaginary parts are plotted as a function of wavenumber in Figure 6. For the unstable wavelengths $s_{+}^{-1}(k)$ is the characteristic time of exponential divergence. The growth rate increases with wavelength, the fastest being the uniform sliding mode, $k=0$, with a growth rate

$$s_m \doteq \alpha\beta \quad (22)$$

Interestingly enough, one can check that $G_{\Gamma}(x, t)$ (12) is readily obtained by summing up both contributions (5) and (18). This differs from previous spectral analysis [*Knopoff et al.*, 2000, eq. 8] where a factor two is missing in front of the I_0 term, due probably to an erroneous computation of the branch cuts contribution. The present derivation demonstrates that the unstable contribution arises only from the poles and that both spectral and boundary integral approaches are indeed fully consistent.

2.3. Dynamics of the Nucleation: scaling behavior

The slip triggered by an impulse load at $x = 0$ behaves as

$$D(x, t) \sim 2\frac{T_0}{\mu}\alpha\beta\frac{e^{\alpha\sqrt{\beta^2 t^2 - x^2}}}{(2\pi\alpha\sqrt{\beta^2 t^2 - x^2})^{1/2}} \quad (23)$$

for $\alpha\sqrt{\beta^2 t^2 - x^2} \gg 1$. As illustrated by numerical simulations in Figure 7, after the nucleation phase the instability takes the form of an expanding zone of high slip velocity, without healing, as in more classical crack models. Nucleation ends when the dynamic strength τ_d , or equivalently the critical slip D_c , is reached somewhere on the fault. The nucleation time T_c is defined as the time needed for slip to reach D_c at the center of the slipping patch. In the limit of long nucleation times, when $\alpha\beta T_c \gg 1$, an implicit

estimation of T_c can be found solving

$$\frac{T_0}{\mu}\frac{\alpha\beta}{\sqrt{2\pi}}\frac{e^{\alpha\beta T_c}}{\sqrt{\alpha\beta T_c}} = D_c \quad (24)$$

Defining $\epsilon \doteq 2\sqrt{2\pi}\Delta\tau/(\alpha^2\beta T_0)$, a parameter that contains the information about the shape of the triggering load, and making use of an expansion of (24) an explicit estimation of T_c can be worked out:

$$T_c \sim s_m^{-1} \{ -\ln(\epsilon) + \ln[\ln(\epsilon)] + \dots \} \quad (25)$$

where s_m was defined in equation (22) as the growth rate of the fastest mode (uniform slip). The dependence on initial conditions is weak, logarithmic. The first order scaling $T_c \sim -s_m^{-1} \ln(\epsilon)$ shows that an estimation of the nucleation time can be deduced from a single mode analysis that retains only the contribution of the fastest mode. Higher order corrections to this scaling arise from the expansion of $\sqrt{\alpha\beta T_c}$ in (24). This square root term reveals an underlying diffusive-like process of importance in the long wavelength limit. Indeed, the growth rate $s_{+}(k)$ of the most unstable modes, $|k| \ll k_c$, can be expanded as

$$s_{+}(k) \sim s_m - \kappa k^2 \quad \text{with} \quad \kappa \doteq \frac{\beta}{2\alpha} \quad (26)$$

To first order, the nucleation is governed by a global exponential divergence with growth rate s_m . To second order, it involves a diffusion process with diffusivity κ . More precisely, if slip is rescaled by its global growth, i.e. if we define $\psi(x, t) \doteq D(x, t)/e^{s_m t}$, the longest wavelengths satisfy asymptotically the diffusion equation

$$\frac{\partial\psi}{\partial t} = \kappa\frac{\partial^2\psi}{\partial x^2} \quad (27)$$

Owing to this analogy we can draw the following remarks: (1) the nucleation triggered by a localized perturbation appears at large scale as a self-similar process, and (2) the slip triggered by a rough perturbation is progressively smoothed.

2.4. Finite size effects

Realistic physical models intrinsically involve a maximum length scale L , which arises from boundary conditions, finite spectrum dynamic triggering or strength heterogeneity distributions. In such cases, the lowest wave number is provided by $k_L = 2\pi/L$. When $k_L = 2\pi/L < k_c$, the fastest growth rate is $s_{+}(k_L) = \beta\sqrt{k_c^2 - k_L^2}$ and the nucleation time scales as

$$T_c \propto s_m^{-1}\frac{L}{\sqrt{L^2 - L_c^2}} \quad (28)$$

where $L_c \doteq 2\pi/\alpha$. This introduces a crossover between two distinct regimes: (1) an infinite fault regime for $L \gg L_c$, where the previous scaling $T_c \propto s_m^{-1}$ holds, and (2) an unconditionally stable regime when $L < L_c$. Finite size effects are important when $L \sim L_c$: the instability involves a critical size

$$L_c = \pi\mu D_c/\Delta\tau \quad (29)$$

and the nucleation time diverges as

$$T_c \propto (L - L_c)^{-\frac{1}{2}} \quad (30)$$

Interestingly enough, one should note that even though in both limits a critical wavenumber k_c exists, it can be related to a critical size only for finite size systems, i.e. when a second length scale is available in the model. In the extreme case of a finite size fault segment,

locked at its tips by infinite strength barriers, the exact critical size has been computed in *Dascalu et al.* [2000] and scales with the L_c reported here.

2.5. Transition to crack-like rupture

As illustrated in Figure 7, the nucleation phase ends with the onset of a crack-like rupture front propagation. The position of the rupture front $X_f(t)$ is here defined to coincide with the fault points where the critical slip D_c is being reached: $D(X_f, t) = D_c$. In a cohesive crack model this definition corresponds to the tail of the process zone. Numerical results based on the BIEM formulation of *Cochard and Madariaga* [1996] show that the rupture front velocity is initially supersonic and approaches the shear wave speed β only asymptotically. This supersonic feature is not nonphysical since, in contrast to classical crack models, the fault is slipping also ahead of the front. Moreover, the rupture front remains inside the causality cone of the initial perturbation.

As the rupture front travels faster than β , the points on and ahead of it can not receive information coming from previous front positions: the evolution of the rupture front does not depend on its own history and it does not perturb the regions ahead, which therefore remain in nucleation and are described by the solution (12). As the asymptotic behavior of slip during the nucleation (23) depends on the conical wave combination, $\sqrt{\beta^2 t^2 - x^2}$, the rupture front describes a hyperbola:

$$t^2 - X_f^2/\beta^2 = T_c^2 \quad (31)$$

The rupture velocity, $V_f(t)$, is given by

$$V_f(t) = \frac{\beta}{\sqrt{1 - T_c^2/t^2}} \quad (32)$$

This solution is consistent with the assumption of supersonicity. As V_f depends on the nucleation time T_c one can expect to retrieve constraints on frictional parameters from the rupture front history. Rupture velocity tends to the shear wave speed but supersonicity is persistent during a time that scales with T_c . Supersonic speed is allowed by the delayed onset of rupture due to the existence of a nucleation phase. The evolution of the rupture front here results from the nucleation process taking place within an extended zone, in contrast to more classical crack models where it is controlled by a local balance at the vicinity of the front, within a small scale process zone, and with no slip outside the crack.

2.6. Behavior out of the fault

As already discussed, the displacement within the bulk, far behind the wave front, decreases exponentially as a function of distance from the fault, with the characteristic length scale α^{-1} . This results from the off-fault behavior of the poles contribution, which controls the dominant part of the nucleation process. From the spectral Green function, equations (13)-(14), the y -dependence of displacement is directly related to $\nu(k, s)$. Its imaginary part is the off-fault wavenumber, while the spatial decay rate is determined by its real part, positive by definition. For each wavenumber k , the poles are defined by $\nu(k, s) = \alpha$. This implies that the nucleation displacement pattern is asymptotically $\propto e^{-|y|/\lambda_\perp}$, where the decay length scale λ_\perp is independent of wavelength:

$$\lambda_\perp = \alpha^{-1} = \frac{\mu}{2\Delta\tau} \times D_c \quad (33)$$

This particular pattern is characteristic of anti-plane shear. However, for other geometries the off-fault displacement is still constrained within a finite width zone surrounding the fault interface. Such a behavior may be interpreted as a *frictional trapping*. Interestingly enough, the geometry of the trapping zone within the bulk,

in particular the trapping depth, provides essential informations on the interface law. In fact, λ_\perp directly scales with D_c , the internal frictional length, with a prefactor that reveals the interplay between the bulk and the interface strengths. This may be used to infer properties of the contact rheology from the deformation measured in the vicinity of the fault interface. Moreover, as will be shown in a latter section, the trapping depth defines a *screening length* for the interactions between the nucleation process on the fault and the heterogeneities of the surrounding materials. A property that has been recently exploited by [*Campillo et al.*, 2001]. In that respect, the fact that this screening length does not depend on the wavenumber is of some importance.

3. A general spectral framework for frictional contact interface

Geophysical applications, in particular the scaling of simulated seismograms, need to bridge the gap toward 3D nucleation models. The spectral linear stability analysis, previously applied to anti-plane shear, can be generalized to other geometries. The basic assumption is the existence of a predefined planar fault Γ , with homogeneous strength properties and uniformly prestressed up to the frictional threshold. The response to an arbitrary load perturbation on Γ involves the Green's function G of the linearized boundary value problem which can be written as the convolution between a bulk propagator \mathcal{P} and an interface Green's function G_Γ :

$$G(k, y, s) = \mathcal{P}(k, y, s) \times G_\Gamma(k, s) \quad (34)$$

The propagator $\mathcal{P}(x, y, t)$ is the displacement perturbation in the surrounding elastic medium due to a unit slip pulse $D(x, t) = \delta(x) \delta(t)$ in an otherwise locked interface. The interface Green's function $G_\Gamma(x, t)$ is the slip perturbation induced by a unit load impulse $T_0(x, t) = \delta(x) \delta(t)$. For instance, in the case of an antiplane geometry, see equation (13), the propagator has a rather simple expression $\mathcal{P}(k, y, s) = 2e^{-\nu y}$. The propagator depends only on the elastic properties of the surrounding medium while the interface Green's function involves also the rheology of the interface. The stability of the system depends therefore only on the interface Green's function.

In general, see Appendix C, the interface Green's function G_Γ can be written in terms of an interface stiffness \mathcal{K} and the frictional parameters of the interface. A boundary stiffness \mathcal{K}_\pm can be defined for each lip of the fault as the response in traction along the boundary of the corresponding half-space due to a unit displacement pulse. In the spectral domain, the interface stiffness can be defined as:

$$\mathcal{K}^{-1}(k, s) = \mathcal{K}_+^{-1}(k, s) + \mathcal{K}_-^{-1}(k, s) \quad (35)$$

The interface stiffness can be split up into tangential \mathcal{K}_\parallel and normal \mathcal{K}_\perp components that can be understood as the elasto-dynamic transfer of shear and normal stresses due to a unit slip pulse. The interface stiffnesses depend on the geometry of the problem, see Appendix C for the case of homogeneous media and *Andrews* [1980]. The frictional parameters involve a frictional weakening γ_\parallel and a normal stress dependence γ_\perp . The interface Green's function can be written as:

$$G_\Gamma(k, s) = [\mathcal{K}_\parallel(k, s) - \gamma_\perp \mathcal{K}_\perp(k, s) - \gamma_\parallel]^{-1} \quad (36)$$

For slip weakening with Coulomb strength threshold, γ_\parallel corresponds to γ used previously, and γ_\perp to the normal stress dependence of the static strength. In the case of rate and rate-and-state

dependent friction laws γ may be itself a function of s [e.g., *Rice and Ruina*, 1983; *Shaw and Rice*, 2000; *Perfettini et al.*, 2000]. Normal coupling is of importance for instance in the case of an interface between two different materials as considered in *Ranjith and Rice* [2000]. When the problem is symmetric with respect to the fault interface, there is no need to consider the normal coupling, $\mathcal{K}_\perp = 0$. To avoid unnecessary notations \mathcal{K} will be used for \mathcal{K}_\parallel . The interface Green's function G_Γ is simply:

$$G_\Gamma(k, s) = [\mathcal{K}(k, s) - \gamma]^{-1} \quad (37)$$

In the 3D case, G_Γ , \mathcal{K} and γ are matrices. In the remaining we only consider two-dimensional cases.

In the s -plane, G_Γ has branch cuts and poles singularities. The branch cuts arise from $\mathcal{K}(k, s)$, which depends generically on $\sqrt{k^2 + s^2/v^2}$ terms, where v stands for each of the wave speeds involved in the problem. Radiation conditions imply that the branch cuts lie on the imaginary axis and therefore only contribute through purely propagative modes. The poles, on the other hand, can lie in the positive real half-plane and control the unstable modes. The poles of G_Γ , in the s plane, can be found by solving, for each k , the following dispersion equation:

$$\mathcal{K}(k, s) = \gamma \quad (38)$$

The instability is generally dominated by the longest wavelengths available in the system. An example of instability dominated by some selected finite length scale can be found in the multi-pulse instability studied by *Lapusta and Rice* [1998] using a specific enhanced weakening rate-and-state law. Quite generally, depending on the parameter $|s/vk|$, two extreme regimes can be identified.

For $|s/vk| \gg 1$, i.e. the high frequency and long wavelength limit, an expansion to second order in $|vk/s|$ gives the *fast limit* of \mathcal{K} :

$$\mathcal{K}(k, s) \sim C(s) s + \Upsilon(s) k^2 \quad (39)$$

The first term can be interpreted as a local radiation damping while the second term can be related to a Laplacian term in space. The nucleation time, in the case of an infinite fault system, scales with the growth rate s_m of the homogeneous mode, the largest root of:

$$C(s)s = \gamma$$

the maximum nucleation growth rate results from the competition between the radiation damping due to the bulk material and the slip weakening rate of the interface friction. It is controlled by a dynamic property if the interface stiffness, more precisely its radiation damping limit. For homogeneous media, the radiation damping coefficient is $C(s) = \mu/2\beta$ and the scaling of the fastest growth rate given by (22) still holds, even in 3D. The diffusion behavior of the longest wavelengths, as illustrated for the anti-plane case (26), can be shown to result from the second leading term in the fast limit expansion. In particular, for in-plane shear the P-SV diffusivity κ is greater than the SH one. In the 3D case the diffusion limit is anisotropic and leads to a macroscopic elliptical shaped slipping patch, with long axis parallel to slip direction, as also seen in numerical experiments [*Favreau*, 2000].

For $|s/vk| \ll 1$, an expansion up to second order in $|s/vk|$ leads to the *slow limit* of the interface stiffness:

$$\mathcal{K}(k, s) \sim K(k) + M(k)s^2 \quad (40)$$

To first order, the static stiffness $K(k)$ is recovered. To second order, each spectral component of slip can be treated as a spring-block system of stiffness $K(k)$ and mass $M(k)$. In anti-plane shear, the

mass is found to be $M(k) = \rho/4|k|$ and can be physically related to the mass mobilized by the static mode of wavenumber k , which induces a deformation into the bulk over a distance $|k|^{-1}$. Similar scalings of the fault mass have been used by *Roy and Marone* [1996] to study the effects of inertia on nucleation, with single degree of freedom systems. For interface laws with an intrinsic length scale, such as the slip weakening and rate-and-state laws, short wavelength are stable and a critical wavenumber k_c defines the boundary between stable and unstable domains of the spectrum. For velocity weakening laws, with no intrinsic length scale, a similar analysis shows that for high velocity weakening rates γ_v , e.g. $\gamma_v > \mu/2\beta$ in anti-plane, all the wavelengths are unstable. For slip weakening laws, $s = 0$ at the stability transition and k_c is defined as the root of:

$$K(k_c) = \gamma$$

The critical wavenumber results here from the competition between two mechanical responses: the *static* elasticity of the material surrounding the fault; the slip weakening rate of the friction that characterized the fault interface. In contrast to s_m , k_c is controlled by the static part of the interface stiffness. Moreover, the spring-mass representation is valid close to k_c . In particular, for a finite size

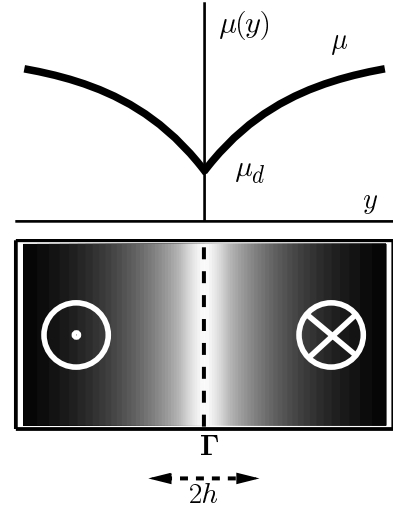


Figure 8. Model of smoothly damaged fault zone FZ1.

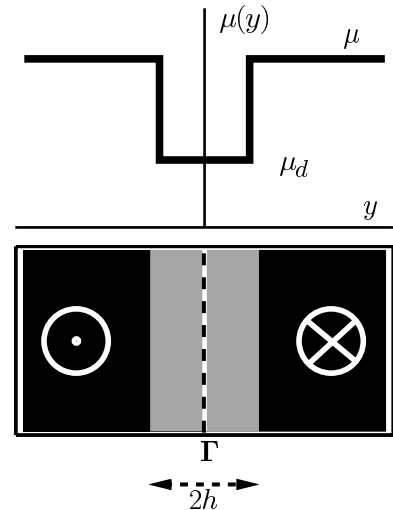


Figure 9. Model of layered damaged fault zone FZ2.

system close to the critical size $L \sim L_c$ this leads to

$$s_m \sim \sqrt{\frac{\gamma - K(k_L)}{M(k_L)}} \propto \sqrt{L - L_c} \quad (41)$$

The exponent $-\frac{1}{2}$ in the scaling (30) of the nucleation time close to the critical size is thus related to the mass like nature of the leading inertial term in the slow limit.

The slow and fast limit, which are shown to be of primary importance during the dynamic nucleation process, are lacking in the so-called quasi-dynamic approximation which only retains the radiation damping and static contributions, $\mathcal{K}(k, s) \equiv \mu s/2\beta + K(k)$. This approximation respects the slow and fast limits only to first order. The first order properties of nucleation, s_m and k_c , will be correctly described but not the second order effects. To explain the diffusion-like scaling of slip and the finite size dynamic effects, inertial effects must be correctly taken into account, even in the slow limit.

4. Simple Anti-Plane models of a Fault zone

As a first step toward more realistic models of the fault zone, interest is focused on anti-plane shearing of two elastic media with variations of the shear velocity β in the direction normal to the fault plane, over a characteristic length scale h . These variations represent a fault-parallel damaged zone of lowered velocity that results from previous rupture history or a localized geological deformation. The geometrical and mechanical properties of the damaged zone are assumed to be stable during the nucleation process. For simplicity the density is that of the surrounding rock, ρ , but the elastic shear modulus is \hat{y} -dependent. Far away from the fault the shear modulus of the intact rock is μ , whereas in the immediate vicinity of the fault it is $\mu_d = (1 - \Delta)\mu$, where $0 < \Delta < 1$ defines the damage level close to the fault. The scale of the fault-parallel damaged zone is given by the characteristic length h of the shear modulus distribution. On the fault plane itself, the interface law is still a linear slip weakening law with weakening rate γ . These fault zone models are therefore defined by four parameters. The two first parameters characterize the undamaged reference model: β , the shear wave velocity of the undamaged elastic material; $\lambda_\perp = \alpha^{-1} = \mu/2\gamma$, the trapping depth of the undamaged fault interface. The two remaining parameters characterize the internal fault zone: Δ , a mechanical property defined as the maximum damage within the fault zone; h , a geometrical property defined as the characteristic width of the damaged fault zone.

In the first fault zone model (FZ1), Figure 8, the shear modulus has a smooth distribution

$$\mu(y) = \mu + (\mu_d - \mu) e^{-|y|/h} \quad (42)$$

In the second fault zone model (FZ2), Figure 9, a layered distribution of the shear modulus is assumed:

$$\mu(y) = \begin{cases} \mu_d & : |y| \leq h \\ \mu & : |y| > h \end{cases} \quad (43)$$

The interface stiffness and the bulk propagator for FZ1 are derived in Appendix D:

$$\mathcal{K}(k, s) = \frac{1}{2}\mu_d \left(\nu + \frac{\Delta}{h} \frac{\mathcal{F}'(a, b; c; \Delta)}{\mathcal{F}(a, b; c; \Delta)} \right) \quad (44)$$

$$\mathcal{P}(k, y, s) = \frac{1}{2} \text{sgn}(y) e^{-\nu|y|} \frac{\mathcal{F}(a, b; c; \Delta e^{-|y|/h})}{\mathcal{F}(a, b; c; \Delta)} \quad (45)$$

where \mathcal{F} is the hypergeometrical function, \mathcal{F}' its derivative with respect to its last argument and

$$\begin{aligned} \nu(k, s) &= \sqrt{k^2 + s^2/\beta^2} \\ a(k, s) &= \frac{1}{2} \left[1 + 2h\nu + \sqrt{1 + (2hk)^2} \right] \end{aligned} \quad (46)$$

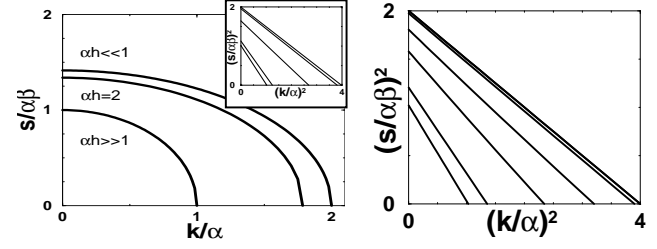


Figure 10. (left) The unstable branch for FZ1, i.e. the positive real valued poles $s_+(k)$ of its interface Green's function $G_\Gamma(k, s)$, as a function of wavenumber k , for $\Delta = 0.5$ and for different values of h . The inset shows s_+^2 as a function of k^2 , for $\alpha h = 0.01, 0.1, 1, 10$ and 100 . The overall shape is elliptical. (right) Same than inset but for FZ2, with $\alpha h = 0.01, 0.1, 0.3, 0.5, 1$ and 10 .

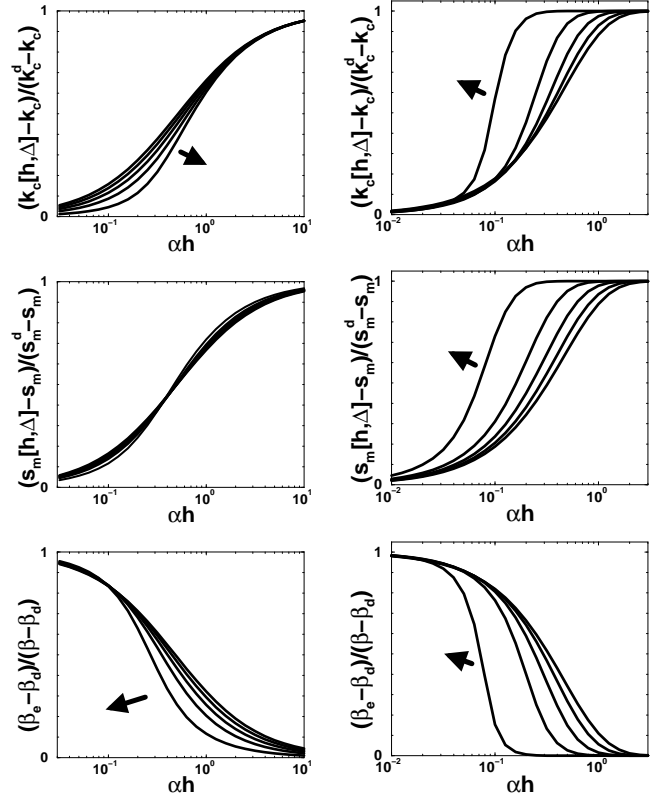


Figure 11. The nucleation and the effective properties as a function of the characteristic width of the fault zone h for two fault zone models: left, model FZ1; right, model FZ2. The characteristic width h is normalized by the trapping depth $\lambda_\perp = \alpha^{-1}$ of the undamaged model. From top to bottom: $\alpha_e = k_c(h, \Delta)$; $s_m(h, \Delta)$ and $\beta_e = s_m(h, \Delta)/k_c(h, \Delta)$. Each curve corresponds to a different value of damage $\Delta = 0.1, 0.3, 0.5, 0.7$ and 0.9 . The arrow shows the trend as damage increases. All the properties $x(h, \Delta)$ are scaled with respect to their limiting values: $x = x(0, \Delta)$, for an undamaged homogeneous medium; $x_d = x(\infty, \Delta)$, for a uniformly damaged medium.

$$b(k, s) = \frac{1}{2} \left[1 + 2h\nu - \sqrt{1 + (2hk)^2} \right]$$

$$c(k, s) = 1 + 2h\nu$$

The interface stiffness and the bulk propagator for FZ2 can be computed by basic elastodynamics in spectral domain:

$$\mathcal{K}(k, s) = \frac{1}{2} \mu_d \nu_d \coth(h\nu_d + \Theta)$$

$$\mathcal{P}(k, y, s) = \begin{cases} \frac{\sinh[\nu_d(h-y) + \Theta]}{2 \sinh(h\nu_d + \Theta)} & : |y| < h \\ \frac{\sinh \Theta}{2 \sinh(h\nu_d + \Theta)} e^{-\nu(y-h)} & : |y| > h \end{cases} \quad (47)$$

where

$$\nu_d(k, s) = \sqrt{k^2 + s^2/\beta_d^2} \quad (48)$$

$$\Theta(k, s) = \operatorname{arctanh} \left(\frac{\mu_d \nu_d}{\mu \nu} \right) \quad (49)$$

The stiffness of the interface between two elastic slabs of width h driven by imposed displacements at their external surface, a case relevant for laboratory simple shear tests, can be obtained as an end member of FZ2 when the outermost medium is rigid, $\mu/\mu_d \rightarrow \infty$. The corresponding interface stiffness is $\mathcal{K}(k, s) = \frac{1}{2} \mu_d \nu_d \coth(\nu_d h)$.

4.1. Stability analysis and nucleation

Interest is focused on the asymptotic behavior of the nucleation for both models of fault zone. As previously shown, asymptotic properties are fully characterized by the unstable poles of the interface Green's function. Numerically, it is found that the evolution of these poles, as a function of wavenumber, can be fitted for both FZ1 and FZ2 models by an ellipse, a quite generic scaling for the anti-plane geometry. Such a scaling is illustrated in Figure 10 and is a robust feature of both models, at least within a reasonable range of damage, $0 < \Delta < 0.9$. The ellipse is completely determined by two properties: the maximum growth rate of the nucleation instability, $s_m(h, \Delta)$, and the critical wavenumber, $k_c(h, \Delta)$, that bounds the unstable spectrum:

$$\frac{s_+^2}{s_m^2(h, \Delta)} + \frac{k^2}{k_c^2(h, \Delta)} = 1 \quad (50)$$

for $|k| \leq k_c(h, \Delta)$. Both properties are obtained numerically by solving the dispersion equation (37) in the fast and slow limits respectively. They fully characterize the asymptotic behavior of fault slip during nucleation.

The dependence of nucleation on the properties of the fault zone can be understood by the scaling of $s_m(h, \Delta)$ and $k_c(h, \Delta)$. Such a scaling is shown for models FZ1 and FZ2 in Figure 11 as a function of h , for a range of damage relevant for the core zone and the outer zone of a fault, $\Delta = 10 - 90\%$. As the trapping depth $\lambda_\perp = \alpha^{-1}$ is the only length scale present in the undamaged reference model, the nucleation in both fault zone models depends on the ratio αh between the characteristic width of the damage distribution and this reference trapping depth. In Figure 11 the governing properties of nucleation are scaled in order to show the continuous crossover between two limiting regimes. For the selected damage levels, the range of αh has been restricted to the transition regime. When $\alpha h \ll 1$, the nucleation process does not depend on the existing damaged fault zone and scales as the previous homogeneous case with the properties of the intact host rock: $k_c(h, \Delta) \rightarrow k_c = \alpha$ and $s_m(h, \Delta) \rightarrow s_m = \alpha\beta$.

When $\alpha h \gg 1$, the nucleation becomes governed by the properties of the damaged material in the immediate vicinity of the fault: $k_c(h, \Delta) \rightarrow k_c^d = \alpha_d$ and $s_m(h, \Delta) \rightarrow s_m^d = \alpha_d \beta_d$, where $\alpha_d^{-1} = \mu_d/2\gamma$ and $\beta_d = \sqrt{\mu_d/\rho}$ are the trapping depth and the shear wave speed in a model of nucleation between two homogeneous damaged half-spaces. In this regime, the nucleation is faster and the unstable spectrum is broader than what would have been estimated using the intact host rock elastic properties alone. Furthermore, the nucleation is no longer dependent on the geometry of the fault zone but only on its mechanical properties. Between these two regimes, a non trivial dependence on the thickness of the fault zone. The main difference between models FZ1 and FZ2 appear in this crossover regime : while the crossover of model FZ1 is weakly dependent on the damage level of the fault zone, the model FZ2 shows a more acute sensitivity on damage.

The crossover for $k_c(h, \Delta)$ allows to define a critical fault zone thickness h^* such that $k_c(h^*, \Delta) = (k_c + k_c^d)/2$. A similar quantity can be defined for the crossover of $s_m(h, \Delta)$. In model FZ1 the critical thickness is found to remain of the same order than λ_\perp , even for strong damage. On the other hand, in the fault zone model FZ2 the critical thickness depends on the damage: h^* decreases as Δ increases, while the transition becomes stiffer and stiffer, as shown in Figure 12 up to extreme values of damage. Such a difference may be related to the different smoothness assumptions in the damage distribution of each model. These two models can be regarded as extreme cases for the damage distribution and provide a glimpse of the complexity that can be expected from realistic fault zones.

In the case of model FZ2, scalings can be analyzed in closed form due to the simpler structure of the interface Green's function and of the propagator. The critical wavenumber $k_c(h, \Delta)$ can be explicitly found by considering in the slow limit the equilibrium between the static stiffness and the weakening rate

$$K(k) = \frac{1}{2} \mu_d |k| \coth(h|k| + \Theta_1) = \gamma \quad (51)$$

where $\Theta_1(\Delta) = \operatorname{arctanh}(1 - \Delta)$. In the long wavelengths limit, $k \ll h^{-1}\Theta_1$, the static stiffness of an homogeneous undamaged medium, $\frac{1}{2}\mu|k|$, is recovered and the critical wavenumber scales as

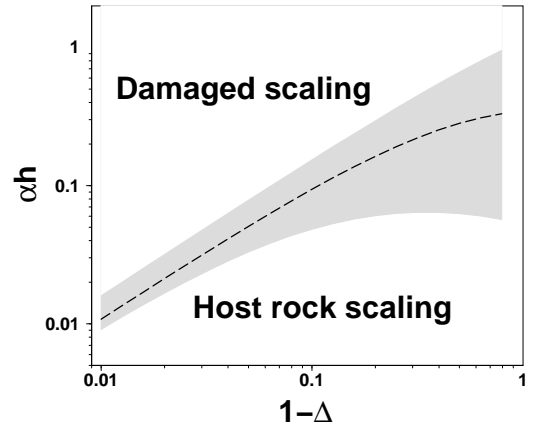


Figure 12. The different scaling regimes of nucleation in model FZ2, as a function of the width of the fault zone, h , and the level of damage, Δ . The gray zone is the transition zone between two extreme regimes, the dashed line gives the critical thickness h^* defined by $k_c(h^*, \Delta) = (k_c + k_c^d)/2$. In thick fault zones the effective properties approach those of an homogeneous damaged medium. Thin fault zones are transparent to the fault. The transition range strongly depends on Δ . Highly damaged fault zones need to be very thin in order to have a negligible effect on nucleation.

$k_c(h, \Delta) \sim \alpha$. In the short wavelengths limit, $k \gg h^{-1}$, the stiffness of a uniformly damaged medium, $\frac{1}{2}\mu_d|k|$, is recovered and the critical wavenumber scales now as $k_c(h, \Delta) \sim \alpha_d$. The critical thickness for the crossover transition of k_c in model FZ2 can be found from (51):

$$h^*(\Delta) = \lambda_{\perp} \frac{1 - \Delta}{1 - \Delta/2} \left[\Theta_1(\frac{1}{2}\Delta) - \Theta_1(\Delta) \right] \quad (52)$$

where $\lambda_{\perp} = \alpha^{-1}$ is the trapping depth of the homogeneous undamaged anti-plane-model. A crossover extension δ^* , related to the steepness of the transition, can be defined as:

$$\delta^*(\Delta) \doteq (\alpha_d - \alpha) / \frac{\partial k_c}{\partial h}(h^*, \Delta) \quad (53)$$

$$= \frac{1}{1 - \Delta/2} \left\{ \frac{1 - \Delta}{1 - \Delta/4} \lambda_{\perp} - h^*(\Delta) \Delta \right\} \quad (54)$$

For weak damage, $\Delta \ll 1$, the critical thickness and the crossover extension scale as $h^*(\Delta) \propto \lambda_{\perp}$ and $\delta^*(\Delta) \propto \lambda_{\perp}$. For strong damage, $\Delta \rightarrow 1$, a situation relevant for the inner gouge zone, the critical fault zone thickness and the crossover extension scale now as the trapping depth of an uniformly damaged anti-plane model, $h^*(\Delta) \propto (1 - \Delta)\lambda_{\perp}$ and $\delta^*(\Delta) \propto (1 - \Delta)\lambda_{\perp}$. The transition sharpens and the critical thickness decreases as the damage increases.

Similar results are found when analyzing the scaling of the growth rate $s_m(h, \Delta)$ which can be explicitly determined, in the case of model FZ2, by considering in the fast limit the equilibrium between the local radiation and the weakening rate:

$$C(s)s = \frac{1}{2}\mu_d \frac{s}{\beta_d} \cotanh(hs/\beta_d + \Theta_2) = \gamma \quad (55)$$

where $\Theta_2(\Delta) = \text{arctanh}(\sqrt{1 - \Delta})$. In fact, comparing (55) to (51), a relation between $s_m(h, \Delta)$ and $k_c(h, \Delta)$ can be found

$$s_m(h, \Delta) = \sqrt{1 - \Delta} \beta k_c(h, 1 - \sqrt{1 - \Delta}) \quad (56)$$

that relates also the critical thickness and the crossover extension of $k_c(h, \Delta)$ and $s_m(h, \Delta)$. The scalings found for the critical wavenumber in the weak and strong damage limits hold therefore also for the maximum growth rate. Now $s_m(h, \Delta)$ and $k_c(h, \Delta)$ being extremal properties of the unstable spectrum, the whole unstable branch, $0 < |k| < k_c(h, \Delta)$, is expected to follow the same trends.

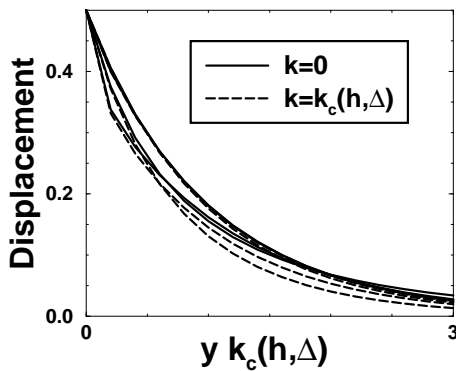


Figure 13. Off-fault displacement of two unstable modes of FZ1, $k = 0$ and $k = k_c(h, \Delta)$, as a function of y for $\Delta = 0.9$ and $\alpha h = 10^{-2}, 10^{-1}, 1$ and 10 . The displacement vanishes exponentially within a distance $k_c^{-1}(h, \Delta)$.

4.2. An effective medium approach

As already discussed, the scaling of the unstable poles as a function of the wavenumber, is quite generic of anti-plane geometry. It follows an ellipse that is defined by two parameters: the maximum growth rate $s_m(h, \Delta)$ and the critical wavenumber $k_c(h, \Delta)$. This ellipse fully characterizes the asymptotic behavior of the slip, for $|k| < k_c(h, \Delta)$, during the nucleation. This suggests that an effective homogeneous model with the same asymptotic nucleation behavior than a damaged fault zone model, characterized by the four parameters $(\alpha, \beta, \Delta, h)$, may be simply defined by two parameters α_e and β_e such that:

$$k_c(h, \Delta) = \alpha_e \quad (57)$$

$$s_m(h, \Delta) = \beta_e \alpha_e \quad (58)$$

These effective parameters are determined on the basis of the scalings of k_c and s_m found for homogeneous models. Interestingly enough, numerical results show that the off-fault deformation in the fault zone model is very well reproduced by the homogenized model. To first-order, displacement remains trapped within a thickness that scales as $\lambda_{\perp}^e = \alpha_e^{-1}$ almost independently of the wavelength, at least for the range of damage, $0 < \Delta < 0.9$, that has been explored, see Figure 13 for model FZ1. This is a non trivial result since, if the asymptotic behavior of slip is completely determined by the shape of the unstable poles branch, the displacement off the fault depends also on the bulk propagator \mathcal{P} which is specific to each fault zone model. From this propagator, it can be shown that, in contrast to the homogeneous anti-plane models, each wavelength has a characteristic trapping depth. However, these trapping depths are only weakly dependent of the wave number and remain all close to λ_{\perp}^e . This shows the pertinence of the proposed homogenization procedure. Departure from this scalings is only expected for extreme values of damage above 90%.

The scalings of the nucleation leading properties, Figure 11, as a function of the characteristic width of the fault zone and the damage can now be analyzed in terms of effective parameters α_e and β_e . The effective trapping depth, $\lambda_{\perp}^e(h, \Delta) = \alpha_e^{-1}$, is bounded by the limiting values obtained for an undamaged and a damaged homogeneous medium, respectively λ_{\perp} and $\lambda_{\perp}^d \doteq \alpha_d^{-1} = (1 - \Delta)\lambda_{\perp}$. In the case of weak damage, these two bounds remain close to each other and therefore $\lambda_{\perp}^e \simeq \lambda_{\perp}$ is a good approximation of the effective trapping depth. For stronger damage $\lambda_{\perp}^d \ll \lambda_{\perp}$ and the effective trapping depth λ_{\perp}^e spans now a broader range of values as h varies. The critical thickness $h^*(\Delta)$, associated with the crossover, can be determined numerically. In all cases, the effective trapping depth can be associated with an off-fault screening effect: the nucleation does not depend on heterogeneities, outside the fault, of scales smaller than the effective trapping depth λ_{\perp}^e . For fault zone model FZ1, the critical thickness was found to remain of the order of λ_{\perp} and it depends only weakly on the damage level. Model FZ1 is therefore characterized by a single off-fault screening length $\simeq \lambda_{\perp}$. This is in contrast to the layered fault zone model FZ2 for which the critical thickness of the crossover exhibits a stronger sensitivity on the damage. In this case, see Figure 12, as the damage increases, the critical thickness decreases and the transition becomes stiffer: the nucleation becomes sensitive to smaller and smaller scales of heterogeneities outside the fault. Frictional trapping is therefore an important phenomenon that controls the nucleation of damaged fault zones. Frictional trapping implies that all the modes see the same effective medium and that arbitrarily long wavelengths can be sensitive to the existence of the fault zone for a thick enough fault zone.

5. Discussion

In general [Chester *et al.*, 1993], a fault zone consists of three structures: a central layer of highly comminuted gouge or ultracataclasite, centimeters to decimeters thick, within a core of foliated

cataclasites, 30 to 100 m thick, embedded in turn in an order of magnitude thicker zone of damaged rock, containing abundant microfractures. The borehole measures across the active Nojima fault, at a depth of about 630 m , showed the presence of a 30 m thick layer of altered and deformed granodiorites surrounding a 20 cm thick gouge layer [Ito *et al.*, 1999]. Inside the gouge zone, high to extreme damage, that can be considered as almost uniform, is expected. Strong and sharp variations of physical properties can be expected at the boundary between the gouge and the surrounding core zone. The core zone in turn can reach damage levels of 50%. In the outer zone, damage decreases continuously with the distance to the fault. However the boundary between the core and the outer zones is difficult to define. Trapped wave inversions usually assume a homogeneous core zone layer while borehole data show a rather smooth distribution of shear wave velocities. The model FZ2 would be appropriate for the gouge, while model FZ1 is more appropriate for the outer zone. Until more precise data is gathered for the core zone, we can not rule out a priori one model or the other.

Figure 12 summarizes the different nucleation behaviors in model FZ2 as a function of the two (geometrical and mechanical) properties defining the fault zone, h and Δ . To assess the effect of each fault zone structure on the nucleation process it is important to estimate the ratio $h/\lambda_{\perp} = \alpha h$ between the trapping depth associated to the host rock and the thickness of the structure considered.

We take as working examples the Nojima fault, which ruptured during the 1995 Kobe earthquake, and the San Andreas system. From waveform inversion of near-field strong motion seismograms [Ide and Takeo, 1997] estimated a 5 MPa stress drop in the hypocentral region of the Kobe earthquake and [Bouchon, 1997] obtained $\Delta\tau \simeq 20 - 100 MPa$ for major Californian earthquakes. As a rule of thumb, the ratio between the reference trapping depth and the critical slip λ_{\perp}/D_c is of the same order than $\mu/\Delta\tau$ and is typically in the range $10^3 - 10^4$. For instance, taking $\mu \approx 43 GPa$, as given by the regional velocity model at the hypocentral depth of the Kobe earthquake, the following scaling for the trapping depth associated with the host rock of Nojima fault is found: $\lambda_{\perp} \approx 4 \times 10^3 \times D_c$.

The value of D_c for real earthquakes is still a matter of discussion. At the laboratory scale it ranges from tens of micrometers for pre-cut surfaces or simulated gouge to some millimeters for fracture of intact granite. Seismological estimates are scattered from some millimeters to some meters [Ohnaka, 2000]. [Aki, 2000] gives for major Californian earthquakes $D_c \approx 0.1 - 1 m$, hence $\lambda_{\perp} \approx 100 m - 10 km$. Due to lack of resolution, [Ide and Takeo, 1997] were only able to give an upper limit, $D_c < 50 cm$, for the deeper part of the Kobe fault, leading to $\lambda_{\perp} < 2 km$. The estimated ranges of h/λ_{\perp} for the three principal fault structures previously defined are summarized in Table 1. This ratio is very low in the case of the gouge zone layer. If model FZ2 is a good description of this layer, high damage ($1 - \Delta = 10^{-6} - 10^{-3}$) is required for the gouge zone to play some role in the effective properties of nucleation. Taking Young's moduli $E = 150 - 500 MPa$ for compact gravel or $E = 10 - 100 MPa$ for sandy material

Table 1. The Ratio $\alpha h = h/\lambda_{\perp}$

| | Gouge zone | Core zone | Outer zone |
|--|---------------------|---------------|--------------|
| Thickness h (in meters) | 0.01 - 0.1 | 10 - 100 | 100 - 10^3 |
| Seismological scaling of αh | $10^{-6} - 10^{-3}$ | $10^{-3} - 1$ | 0.01 - 10 |
| laboratory scaling of αh | 0.01 - 0.1 | 1 - 10^3 | 10 - 10^4 |

and Poisson's ratio $\nu = 0.3$, contrasts in shear moduli of two to four orders of magnitude are expected at the boundary between the gouge zone and the surrounding core. Thus in general this zone is not seen by the fault during nucleation, unless its shear modulus is extremely low, i.e. a practically fluidized layer. The issue of the role of the core zone and outer zone is less clear. Although there is a trend toward an intact host rock scaling of nucleation, an effect can still be possible for short D_c , high stress drop or relatively thin fault structure.

However, complex interactions during fast dynamic rupture can lead to apparent values of D_c larger than the local D_c [Yamashita and Fukuyama, 1996]. The relevance of these large apparent values for nucleation remains an open question. An alternative insight can be reached from laboratory experiments. On the basis of experimental data on simulated gouge zones [Marone and Kilgore, 1993] proposed the scaling $D_c \approx 0.01 \times h_{gouge}$, where h_{gouge} is the gouge layer thickness. If this scaling is extrapolated to real earthquakes it gives

$$\lambda_{\perp} \approx 10 - 100 \times h_{gouge} \quad (59)$$

For Nojima fault it results that $\lambda_{\perp} \simeq 8 m$, for faults in the San Andreas system $\lambda_{\perp} \approx 0.1 - 10 m$. The ratio h/λ_{\perp} based on this scaling for the different typical internal structures of a fault zone are reported in the last row of Table 1.

If the gouge layer is described by model FZ2 then the shear modulus contrast must be higher than 90 - 99 % for the layer to have some effect on nucleation. This range is clearly below the range of contrasts for mature gouge zones. The gouge is thus expected to play a role not only by its geometry, that controls D_c , but also by its elastic properties.

More than 50% decrease in wave velocities was measured in the Nojima core zone. For those levels of damage ($\Delta > 0.75$) the fault core need to be thicker than $\lambda_{\perp}^c \simeq 0.25 \times \lambda_{\perp}$ in order to have some effect on the nucleation process. The effective trapping depth is $\lambda_{\perp}^c \approx 2 m$ for Nojima and $\lambda_{\perp}^c \approx 2.5 cm - 2.5 m$ for San Andreas if (59) holds. If we take model FZ1 instead, the screening length is of order λ_{\perp} . The core zone is 30 m thick in the shallow section of Nojima fault and 30 - 100 m thick in some faults of the San Andreas system. More generally, the core zone being usually at least two orders of magnitude thicker than the gouge zone, (59) implies that this structure is clearly thicker than the relevant screening length, whichever model of fault zone is considered. This in turn implies (1) that nucleation is prone to scale like in a homogeneous medium, with the mechanical properties of the fault core zone, and (2) that the geometrical details of the distribution of damage at his mesoscopic scale are not significant. It leads to faster nucleation growth and broader unstable spectra than expected from the host intact rock scaling.

Measures from the exhumed Punchbowl and San Gabriel faults of the San Andreas system [Chester *et al.*, 1993] give an average thickness of 300 - 1000 m for the outer fault zone. Although this is thick enough for the fault to see it, the lower overall damage and smoother distribution inside this outer region makes it likely to be screened by the core zone effects.

Actually the range of values for the internal friction length D_c , during the nucleation phase, is nowadays poorly constrained. Furthermore, a physical understanding of the difference between laboratory and seismological estimations is still lacking. Such an uncertainty leads to a wide range of possible nucleation regimes. This suggest that additional observations directly related to the nucleation process would be most useful.

Nucleation phases are not easily observed in current seismograms. Even when observed, a nucleation time is difficult to define

objectively. Moreover, it will not be directly related to the nucleation time studied here. In fact T_c is of little practical interest due to the type of triggering of this kind of studies and due also to the noise level that should prevent a direct measure from the seismograms. A well defined observable quantity is in fact s_m , the maximum growth rate. Indeed, the rate of the seismic moment, which can be measured on the far field, is related to the spectral component $k = 0$ through $M_0(t) \propto D(k=0, t)$. Owing to the radiation damping limit for 3D elastodynamics in homogeneous media, the model predicts $D(k=0, t) \propto e^{s_m t}$, with $s_m = \alpha_e \beta_e$. Therefore, the maximum growth rate could be measured by plotting

$$s_m = \dot{M}_0(t)/M_0(t) \quad (60)$$

for the initial phase of the seismogram. This could help to constrain the frictional properties of the fault and the effective properties of the fault zone. However, one should keep in mind that such an exponential behavior is not generic and that other nucleation models can predict power law scalings instead [Sato and Kanamori, 1999]. Different scalings may be expected also for dynamic triggering well below the sliding threshold, or for sophisticated nucleation models that take into account possible heterogeneities of initial stress or friction threshold.

6. Conclusion

The nucleation of the rupture has been solved for simple models of fault zone using a linearized perturbation analysis. The fault interface behavior is assumed to obey a simple linear slip weakening law. In such an analysis, the fault is initially uniformly stressed at sliding threshold. This reference state is more a mathematical ersatz than a realistic physical condition. However, this allows for analytical solutions that are quite useful in providing physical insights on the nucleation process and reference solutions for more elaborated numerical analysis.

In the simple case of an anti-plane shear between two homogeneous elastic half-space, both space-time and spectral solution have been independently obtained and shown to be fully consistent. The spectral framework has been extended to discuss implications on 3D rupture. The nucleation is characterized by: a bounded spectrum of unstable modes with a critical wavenumber k_c ; a time exponential growth of the unstable modes with a maximum rate s_m ; an induced off-fault deformation that remains trapped within a bounded zone in the vicinity of the fault with a characteristic depth penetration λ_\perp . All these physical parameters have been explicitly related to the slip weakening rate at the fault interface and to the elastic property of the surrounding medium.

Internal fault zone structures have been taken into account here in terms of fault-parallel damaged zones. Spectral solutions have been obtained for both a smooth and a layered distribution of damage. A crossover is observed between a regime of intact rock scaling and a regime of homogeneously damaged material. The properties of this transition are shown to depend on the smoothness of the damage distribution inside the fault zone. Moreover, it is shown that the nucleation process of damaged fault zones can be correctly described in terms of an effective homogeneous model characterized by two effective parameters: an effective shear wave velocity β_e and an effective nucleation length α_e^{-1} . In all cases, the frictional trapping of the deformation off the fault is of crucial importance. Generally the effective properties of an heterogeneous medium are scale dependent. For instance, one expects them to depend on the wavelength considered. However due to frictional trapping of the deformation out of the fault, all the modes “see” the same effective medium and, beyond a critical thickness of a fault zone, even arbitrarily long wavelengths can be sensitive to the existence of the fault zone.

The importance of the different structures of real fault zones in the nucleation process has been discussed. Conclusions are quite dependent on the admissible range for the critical slip D_c . Seismological estimates predict low sensitivity to the fault zone, although significant effects of the core and outer zones are expected for short D_c , high stress drop or relatively thin fault structure. When laboratory based scalings are used, the fault core zone is predicted to play an essential role, leading to a fast nucleation growth, broad unstable spectrum and a highly localized deformation. Such mismatch should be resolved in the near future with the help of forthcoming borehole data across active faults.

The most important prediction of our model is the existence of a frictional trapping length, that determines the effective properties of the fault zone. This relies on the assumption of an internal length for the friction law. We therefore expect that this study can be extended beyond the slip weakening case. Such an extension deserves more precise experiments and further scrutiny.

Appendix A: Getting w from Φ

Laplace transforming equation (5) with respect to y , noting with a tilde the transformed quantities and p the transform variable:

$$p\tilde{\Psi}(x, p, t) - \Psi(x, 0, t) = (\alpha + p) \tilde{w}(x, p, t) - w(x, 0, t) \quad (A1)$$

For $p = -\alpha$, we get

$$w(x, 0, t) = \Psi(x, 0, t) + \alpha \tilde{\Psi}(x, -\alpha, t) \quad (A2)$$

This leads directly to the representation of fault slip as in (10). To get the displacement field everywhere in the bulk, we replace (A2) into (A1) and rearrange the resulting expression as

$$\tilde{w}(x, p, t) = \tilde{\Psi}(x, p, t) - \frac{\alpha}{\alpha + p} [\tilde{\Psi}(x, p, t) - \tilde{\Psi}(x, -\alpha, t)] \quad (A3)$$

Going back to y domain, noting that the inverse Laplace transform of $\frac{1}{\alpha+p}$ is $H(y) e^{-\alpha y}$, we obtain the solution (9) for the displacement in the whole elastic space.

Appendix B: Spectral derivation of the Green’s function

Applying a Fourier transform in x and one-sided Laplace transform in y and t with the corresponding transformed variables k , p and s , the wave equation gives

$$\frac{s^2}{\beta^2} \tilde{w}(k, p, s) = (p^2 - k^2) \tilde{w}(k, p, s) - p w(k, y=0, s) - \frac{\partial w}{\partial y}(k, y=0, s) \quad (B1)$$

The last term can be replaced by the fault boundary condition, $-\frac{\partial w}{\partial y}(k, y=0, s) = T_0(k, s)/\mu + \alpha w(k, y=0, s)$. Equation (B0) becomes

$$(\nu^2 - p^2) \tilde{w}(k, p, s) = (\alpha - p) w(k, y=0, s) + \frac{T_0(k, s)}{\mu} \quad (B2)$$

For $p = \nu$, we get the displacement of the lip of the fault, which is half the slip

$$w(k, y=0, s) = \frac{T_0(k, s)}{\mu(\nu - \alpha)} \quad (B3)$$

From this expression we deduce the interface Green's function $G_\Gamma(k, s)$ (15). Replacing (B3) in (B2) we get the displacement inside the bulk:

$$\tilde{w}(k, p, s) = \frac{T_0(k, s)}{\mu(\nu + p)(\nu - \alpha)} \quad (\text{B4})$$

Back transforming to the y domain leads to

$$w(k, y, s) = \frac{T_0(k, s) e^{-\nu y}}{\mu(\nu - \alpha)} \quad (\text{B5})$$

and to the Green's function $G(k, y, s)$ (14). To transform it back to (x, t) domain we start by rearranging it:

$$G(k, y, s) = \frac{1}{\nu} \times \frac{e^{-\nu y}}{\mu} \left(1 + \frac{\alpha}{\nu - \alpha} \right) \quad (\text{B6})$$

Making use of [Erdélyi et al., 1954, 5.1.6]

$$\mathcal{L}^{-1} \left\{ \frac{1}{\nu} \times \tilde{f}(\nu) \right\} = \beta \int_0^{\beta t} J_0 \left[|k| \sqrt{\beta^2 t^2 - \xi^2} \right] f(\xi) d\xi \quad (\text{B7})$$

and of the backward transform $f(\xi) = \delta(\xi - y) + \alpha e^{\alpha(\zeta - y)}$ of $\tilde{f}(p) = e^{-py} (1 + \frac{\alpha}{p - \alpha})$, we obtain an expression in (k, t) domain

$$G(k, y, t) = \frac{\beta}{\mu} J_0(|k| \sqrt{\beta^2 t^2 - y^2}) + \frac{\alpha\beta}{\mu} e^{-\alpha y} \int_y^{\beta t} J_0 \left(|k| \sqrt{\beta^2 t^2 - \zeta^2} \right) e^{\alpha\zeta} d\zeta \quad (\text{B8})$$

Noting that $(\beta/\mu)J_0(\beta|k|t)$ is the Fourier transform with respect to x of Lamb's solution, we can transform back to x domain and get (9).

The poles contribution can be transformed back following the same technique. Writing it in the form $G_p(k, s) = \frac{1}{\nu} \times \frac{4\alpha}{\mu} \frac{\nu}{\nu^2 - \alpha^2}$ one can use (B7) to transform it back to t domain

$$G_p(k, t) = \frac{4\alpha\beta}{\mu} \int_0^{\beta t} J_0 \left[|k| \sqrt{\beta^2 t^2 - \xi^2} \right] \cosh(\alpha\xi) d\xi \quad (\text{B9})$$

Transforming back to x domain inside the integral:

$$G_p(x, t) = \frac{4\alpha\beta}{\mu} \int_0^{\sqrt{\beta^2 t^2 - x^2}} \frac{\cosh(\alpha\xi)}{\pi \sqrt{\beta^2 t^2 - x^2 - \xi^2}} d\xi \quad (\text{B10})$$

The final result (18) can be inferred using the following integral representation of the modified Bessel function of zeroth order

$$I_0(z) = 2 \int_0^1 \frac{\cosh(z\xi)}{\pi \sqrt{1 - \xi^2}} d\xi \quad (\text{B11})$$

Appendix C: Interface stiffness for homogeneous medium

Defining $\nu_S(k, s) \doteq \sqrt{k^2 + s^2/\beta^2}$ and $\nu_P(k, s) \doteq \sqrt{k^2 + s^2/\nu_P^2}$, where ν_P is the P-wave speed of the medium, the interface stiffness and the bulk propagators for anti-plane shear (SH) and in-plane shear (P-SV) are

$$\mathcal{K}_{SH}(k, s) = \frac{1}{2} \mu \nu_S \quad (\text{C1})$$

$$\mathcal{P}_{SH}(k, y, s) = \pm \frac{1}{2} e^{-\nu_S |y|} \quad (\text{C2})$$

$$\mathcal{K}_{PSV}(k, s) = 2\mu \left(\frac{k\beta}{s} \right)^2 (\nu_S - \nu_P) + \mu \frac{s^2/\beta^2}{2\nu_S} \quad (\text{C3})$$

$$\mathcal{P}_{PSV}^x(k, y, s) = \pm \frac{1}{2} e^{-\nu_S |y|} \pm \left(\frac{\beta k}{s} \right)^2 (e^{-\nu_S |y|} - e^{-\nu_P |y|}) \quad (\text{C4})$$

$$\mathcal{P}_{PSV}^y(k, y, s) = i \frac{k}{\nu_S} \left\{ \frac{1}{2} e^{-\nu_S |y|} + \left(\frac{\beta k}{s} \right)^2 \times \left(e^{-\nu_S |y|} - \frac{\nu_S \nu_P}{k^2} e^{-\nu_P |y|} \right) \right\} \quad (\text{C5})$$

where \pm in the propagators stand for the $y > 0$ and $y < 0$ half spaces. For a plane fault in a 3D elastic medium, with fixed slip direction parallel to \hat{z} , we define the wavenumber vector $\mathbf{k} = (k, \theta)$ by its modulus $k > 0$ and the angle $\theta \in [0, 2\pi]$ between \mathbf{k} and \hat{x} . The interface stiffness and the bulk propagator are

$$\mathcal{K}(\mathbf{k}, s) = \cos^2 \theta \mathcal{K}_{PSV} + \sin^2 \theta \mathcal{K}_{SH} \quad (\text{C6})$$

$$\mathcal{P}^x(\mathbf{k}, y, s) = \cos^2 \theta \mathcal{P}_{PSV}^x + \sin^2 \theta \mathcal{P}_{SH} \quad (\text{C7})$$

$$\mathcal{P}^y(\mathbf{k}, y, s) = \cos \theta \mathcal{P}_{PSV}^y \quad (\text{C8})$$

When the slip direction is arbitrary, the interface stiffness is a matrix relating both components of traction to slip (D_x, D_z):

$$\mathcal{K}(\mathbf{k}, s) = \mathcal{R}_\theta^T \begin{pmatrix} \mathcal{K}_{PSV}(k, s) & \\ & \mathcal{K}_{SH}(k, s) \end{pmatrix} \mathcal{R}_\theta \quad (\text{C9})$$

where \mathcal{R}_θ is the θ -rotation matrix:

$$\mathcal{R}_\theta = \begin{pmatrix} \cos \theta & \sin \theta \\ -\sin \theta & \cos \theta \end{pmatrix} \quad (\text{C10})$$

The propagator for the components u_x and u_z of displacement is

$$\mathcal{P}^{xz}(\mathbf{k}, y, s) = \mathcal{R}_\theta^T \begin{pmatrix} \mathcal{P}_{PSV}^x & \\ & \mathcal{P}_{SH} \end{pmatrix} \mathcal{R}_\theta \quad (\text{C11})$$

The propagator for the component u_y is

$$\mathcal{P}^y(\mathbf{k}, y, s) = \mathcal{P}_{PSV}^y \begin{pmatrix} \cos \theta \\ \sin \theta \end{pmatrix} \quad (\text{C12})$$

Appendix D: Interface stiffness for a damaged fault zone

The governing equation for displacement $w(x, y, t)$ in the anti-plane case with non homogeneous elastic modulus $\mu(y)$ is

$$\rho \frac{\partial^2 w}{\partial t^2} = \mu(y) \frac{\partial^2 w}{\partial x^2} + \frac{\partial}{\partial y} \left(\mu(y) \frac{\partial w}{\partial y} \right) \quad (\text{D1})$$

To get the interface stiffness, we must apply the boundary condition

$$w(x, 0, t) = \frac{1}{2} \delta(x) \delta(t) \quad (\text{D2})$$

and conditions of bounded displacement at $y = \pm\infty$. The boundary problem for $w(k, y, s)$

$$(\rho s^2 + \mu k^2) w - \frac{\partial}{\partial y} \left(\mu \frac{\partial w}{\partial y} \right) = 0 \quad (\text{D3})$$

$$w(k, 0, s) = 1/2 \quad (\text{D4})$$

$$w(k, \pm\infty, s) = O(1) \quad (\text{D5})$$

can be solved numerically for any arbitrary distribution $\mu(y)$, and any given (k, s) . The interface stiffness is then computed from the traction at Γ : $\mathcal{K}(k, s) = -\mu(0) \frac{\partial w}{\partial y}(k, 0, s)$. However, for model FZ1 an analytical solution can be derived. We seek solutions of the form:

$$w(k, y, s) = \frac{1}{2} Y(k, y, s) e^{-\nu|y|} \quad (\text{D6})$$

where $\nu = \sqrt{k^2 + s^2/\beta^2}$ is defined to have a positive real part, and β is the shear wave velocity far away from the fault. The exponential term accounts for the behavior of the solution far away from the damaged zone which asymptotically approaches the solution of an intact infinite space. From now on we fix k and s and for the sake of clearness we drop the Y dependence on (k, s) . Applying the following variable change [Vrettos, 1990]:

$$\xi = \Delta \exp\left(-\frac{|y|}{h}\right) \quad (\text{D7})$$

we get the following scalar differential equation for $Y(\xi)$:

$$(1 - \xi)\xi Y'' + [2r + 1 - 2(r + 1)\xi] Y' - (\Omega^2 + r) Y = 0 \quad (\text{D8})$$

where the dimensionless coefficients are

$$\begin{aligned} r &= h\nu \\ \kappa &= hk \\ \Omega &= hs/\beta \end{aligned}$$

and the boundary conditions are

$$\begin{aligned} Y(\xi) &= o(\xi^r) \\ Y(\Delta) &= 1 \end{aligned} \quad (\text{D9})$$

Equation (D8) is actually an hyper-geometric differential equation,

$$(1 - \xi)\xi Y'' + [c - (a + b + 1)\xi] Y' - ab Y = 0 \quad (\text{D10})$$

with

$$\begin{aligned} a &= \frac{1}{2} \left[1 + 2r + \sqrt{1 + 4\kappa^2} \right] \\ b &= \frac{1}{2} \left[1 + 2r - \sqrt{1 + 4\kappa^2} \right] \\ c &= 1 + 2r \end{aligned}$$

The solution of (D10) with boundary conditions (D9) is related to the hyper-geometric function,

$$\mathcal{F}(a, b; c; \xi) = \sum_{n=0}^{\infty} \frac{(a)_n (b)_n}{(c)_n n!} \xi^n$$

by:

$$Y(\xi) = \frac{\mathcal{F}(a, b; c; \xi)}{\mathcal{F}(a, b; c; \Delta)} \quad (\text{D11})$$

The traction at the interface, $-\mu_d \partial w / \partial y(k, 0, s)$, gives the interface stiffness:

$$\mathcal{K}(k, s) = (1 - \Delta) \mathcal{K}_{\infty}(k, s) + \frac{1}{2} \mu_d \frac{\Delta}{h} \frac{\mathcal{F}'(a, b; c; \Delta)}{\mathcal{F}(a, b; c; \Delta)} \quad (\text{D12})$$

where \mathcal{F}' is the derivative of the hyper-geometric function with respect to its last argument, ξ , and $\mathcal{K}_{\infty}(k, s) = \frac{1}{2} \mu \nu$ is the inter-

face stiffness in the homogeneous case, which is recovered when $\Delta = 0$.

Acknowledgments. The authors wish to acknowledge enlightening discussions with R. Madariaga, I. Main and M. Campillo. We also thank L. Knopoff for fruitful discussion on the preprint version of Knopoff *et al.* [2000] during his visit at IPGP last July. We benefit from the detailed and constructive review of an anonymous reviewer. This work has been partially supported by the PNRN Program of the CNRS, by the ACI "Risques naturels" of the MENRT, and by DGPA-UNAM under grant IN104998.

References

- Aki, K., Scale-dependence in earthquake processes and seismogenic structures, *Pure appl. geophys.*, *157*, 2249–2258, 2000.
- Andrews, D., Rupture propagation with finite stress in antiplane strain, *J. Geophys. Res.*, *81*, 3575–3582, 1976.
- Andrews, D., Fault impedance and earthquake energy in the Fourier transform domain, *Bull. Seism. Soc. Am.*, *70*, 1683–1698, 1980.
- Andrews, D., and Y. Ben-Zion, Wrinkle-like slip pulse on a fault between different materials, *J. Geophys. Res.*, *102*, 553–571, 1997.
- Ben-Zion, Y., Properties of seismic fault zone waves and their utility for imaging low-velocity structure, *J. Geophys. Res.*, *103*, 12,567–12,585, 1998.
- Ben-Zion, Y., and K. Aki, Seismic radiation from an SH line source in a laterally heterogeneous planar fault zone, *Bull. Seismol. Soc. Am.*, *80*, 971–994, 1990.
- Beroza, G., and W. Ellsworth, Properties of the seismic nucleation phase, *Tectonophysics*, *261*, 209–227, 1996.
- Bouchon, M., The state of stress on some faults of the San Andreas system as inferred from near-field strong motion data, *J. Geophys. Res.*, *102*, 11,731–11,744, 1997.
- Campillo, M., and I. Ionescu, Initiation of antiplane shear instability under slip dependent friction, *J. Geophys. Res.*, *102*, 20,363–20,371, 1997.
- Campillo, M., P. Favreau, I. Ionescu, and C. Voisin, On the effective friction of a heterogeneous fault, *J. Geophys. Res.*, *106*, 16,307–16,322, 2001.
- Chester, F., J. Evans, and R. Biegel, Internal structure and weakening mechanisms of the San Andreas fault, *J. Geophys. Res.*, *98*, 771–786, 1993.
- Cochard, A., and R. Madariaga, Complexity of seismicity due to highly rate-dependent friction, *J. Geophys. Res.*, *101*, 25,321–25,336, 1996.
- Cochard, A., and J. Rice, Fault rupture between dissimilar materials: Ill-posedness, regularization, and slip-pulse response, *J. Geophys. Res.*, *2000*, in press.
- Dascalu, C., I. Ionescu, and M. Campillo, Fault finiteness and initiation of dynamic shear instability, *Earth Planet. Sci. Lett.*, *177*, 163–176, 2000.
- Dieterich, J., Preseismic fault slip and earthquake prediction, *J. Geophys. Res.*, *83*, 3940–3948, 1978.
- Dieterich, J., Potential for geophysical experiments in large scale tests, *Geophys. Res. Lett.*, *8*, 653–656, 1981.
- Dieterich, J., Earthquake nucleation on faults with rate- and state-dependent strength, *Tectonophysics*, *211*, 115–134, 1992.
- Dieterich, J., and B. Kilgore, Implications of fault constitutive properties for earthquake prediction, *Proc. Natl. Acad. Sci. USA*, *93*, 3787–3794, 1996.
- Dieterich, J., D. Barber, G. Conrad, and Q. Gorton, Preseismic slip in a large scale friction experiment, *Proc. U.S. Symp. Rock Mech*, *19*, 110–117, 1978.
- Dodge, D., G. Beroza, and W. Ellsworth, Foreshock sequence of the 1992, Landers, California earthquake and its implications for earthquake nucleation, *J. Geophys. Res.*, *100*, 9865–9880, 1995.
- Dodge, D., G. Beroza, and W. Ellsworth, Detailed observations of California foreshock sequences: Implication for the earthquake process., *J. Geophys. Res.*, *101*, 22,371–22,392, 1996.
- Ellsworth, W., and G. Beroza, Seismic evidence for a seismic nucleation phase, *Science*, *268*, 851–855, 1995.
- Ellsworth, W., and G. Beroza, Observation of the seismic nucleation phase in the Ridgecrest, California, earthquake sequence, *Geophys. Res. Lett.*, *25*, 401–404, 1998.
- Erdélyi, A., W. Magnus, F. Oberhettinger, and F. Tricomi (Eds.), *Tables of integral transforms*, vol. I of the *Bateman Manuscript Project*, McGraw-Hill, New York, 1954.
- Favreau, P., Initiation et propagation de la rupture sismique : instabilité de frottement en elastodynamique, Ph.D. thesis, Univ. Grenoble I, 2000.

- Favreau, P., M. Campillo, and I. Ionescu, Initiation of in-plane shear instability under slip-dependent friction, *Bull. Seismol. Soc. Am.*, 89, 1280–1295, 1999.
- Favreau, P., M. Campillo, and I. Ionescu, Initiation of shear instability in 3d, *Geophys. J. Int.*, 2000, submitted.
- Fukao, Y., and B. Shibazaki, Is the eventual size of earthquake determined by the mode of earthquake nucleation, *Kagaku*, 65, 211–218, 1995.
- Gradshteyn, I., and I. Ryzhik, *Table of integrals, series and products*, Academic Press, New York and London, 1965.
- Harris, R., and S. Day, Effects of a low-velocity zone on a dynamic rupture, *Bull. Seism. Soc. Am.*, 87, 1267–1280, 1997.
- Ide, S., and M. Takeo, Determination of constitutive relations of fault slip based on seismic wave analysis, *J. Geophys. Res.*, 102, 27,379–27,391, 1997.
- Iio, Y., Slow initial phase of the p-wave velocity pulse generated by microearthquakes., *Geophys. Res. Lett.*, 19, 1992.
- Iio, Y., Observations of the slow initial phase generated by microearthquakes: implications for earthquake nucleation and propagation, *J. Geophys. Res.*, 100, 15,333–15,349, 1995.
- Iio, Y., et al., Slow initial phase generated by microearthquakes occurring in the Western Nagano prefecture, Japan - the source effect, *Geophys. Res. Lett.*, 26, 1969–1972, 1999.
- Ionescu, I., and M. Campillo, Influence of the shape of friction law and fault finiteness on the duration of initiation, *J. Geophys. Res.*, 104, 3013–3024, 1999.
- Ishira, Y., Y. Fukao, I. Yamada, and H. Aoki, Rising slope of moment rate functions: the 1989 earthquakes off east coast of Honshu, *Geophys. Res. Lett.*, 19, 873–876, 1992.
- Ito, H., Y. Kuwahara, T. Kiguchi, K. Fujimoto, and T. Ohtani, Outline of the Nojima fault drilling by GSJ: structure, physical properties and permeability structure from borehole measurements in GSJ borehole crossing the Nojima fault, Japan, in *International workshop on the Nojima fault core and borehole data analysis*, 1999.
- Kato, N., and T. Hirasawa, A numerical study on seismic coupling along subduction zones using a laboratory-derived friction law, *J. Geophys. Res.*, 102, 3427–3434, 1997.
- Knopoff, L., J. Landoni, and M. Abinante, The causality constraint for fractures with linear slip-weakening, *Geophys. J. Int.*, 2000, in press.
- Lapusta, N., and J. Rice, Complex multi-pulse mode of rupture propagation, in *EOS Trans. Amer. Geophys. Union*, vol. 79 of *Fall Meeting Supplement*, p. F622., 1998.
- Lapusta, N., J. Rice, Y. Ben-Zion, and G. Zheng, Elastodynamic analysis for slow tectonic loading with spontaneous rupture episodes on faults with rate- and state-dependent friction, *J. Geophys. Res.*, 2000, in press.
- Li, Y., and P. Leary, Fault-zone trapped seismic waves, *Bull. Seismol. Soc. Am.*, 80, 1245–1271, 1990.
- Li, Y., and J. Vidale, Low-velocity fault zone guided waves: Numerical investigations of trapping efficiency, *Bull. Seismol. Soc. Am.*, 86, 371–378, 1996.
- Li, Y., K. Aki, J. Vidale, and F. Xu, Shallow structure of the Landers fault zone from explosion-generated trapped waves, *J. Geophys. Res.*, 104, 20,257–20,275, 1999.
- Marone, C., Laboratory-derived friction laws and their application to seismic faulting, *Annu. Rev. Earth Planet. Sci.*, 26, 643–696, 1998.
- Marone, C., and B. Kilgore, Scaling of the critical slip distance for seismic faulting with shear strain in fault zones., *Nature*, 362, 618–621, 1993.
- Matsu'ura, M., H. Kataoka, and B. Shibazaki, Slip-dependent friction law and nucleation processes in earthquake rupture, *Tectonophysics*, 211, 135–148, 1992.
- Michelini, A., and T. McEvelly, Seismological studies at Parkfield, I. Simultaneous inversion for velocity structure and hypocenter using cubic B-splines parametrization, *Bull. Seismol. Soc. Am.*, 81, 524–552, 1991.
- Mori, J., and H. Kanamori, Rupture initiations of microearthquakes in the 1995 Ridgecrest, California sequence, *Geophys. Res. Lett.*, 23, 2437–2440, 1996.
- Ohnaka, M., Dynamic breakdown processes and the generating mechanism for high frequency elastic radiation during stick-slip instabilities., in *Earthquakes Source Mechanics*, edited by S. Das, J. Boatwright, and C. Scholz, vol. 24, union monogr. ed., pp. 13–24, Am. Geophys. Union, Washington, DC, 1986.
- Ohnaka, M., Nonuniformity of the constitutive law parameters for shear rupture and quasistatic nucleation to dynamic rupture: a physical model of earthquake generation processes, *Proc. Natl. Acad. Sci. U.S.A.*, 93, 3795–3802, 1996.
- Ohnaka, M., A physical scaling relation between the size of an earthquake and its nucleation zone size, *Pure appl. geophys.*, 157, 2259–2282, 2000.
- Ohnaka, M., and L. Shen, Scaling of the shear rupture process from nucleation to dynamic propagation : implications of geometric irregularity of the rupturing surfaces, *J. Geophys. Res.*, 104, 817–844, 1999.
- Ohnaka, M., and K. Yamamoto, Experimental studies of failure nucleation and propagation along simulated faults in rock, study on short-period behavior in fault motion and estimation of input seismic motion, in *Final Tech. Rep A-59-3*, edited by R. Sato, pp. 11–46, Univ. Tokyo, Tokyo, 1984.
- Ohnaka, M., and T. Yamashita, A cohesive zone model for dynamic shear faulting based on experimentally inferred constitutive relation and strong motion source parameters, *J. Geophys. Res.*, 94, 4089–4104, 1989.
- Ohnaka, M., Y. Kuwahara, and K. Yamamoto, Nucleation and propagation processes of stick-slip failure and normal stress dependence of the physical parameters of dynamic slip failure, *J. Nat. Disaster Sci.*, 9, 121, 1987a.
- Ohnaka, M., Y. Kuwahara, and K. Yamamoto, Constitutive relations between dynamic physical parameters near a tip of the propagating slip zone during stick-slip shear failure, *Tectonophysics*, 144, 109–125, 1987b.
- Okubo, P., and J. Dieterich, Effects of physical fault properties on frictional instabilities produced on simulated faults, *J. Geophys. Res.*, 89, 5817–5827, 1984.
- Perfettini, H., J. Schmittbuhl, J. Rice, and M. Cocco, Fault response induced by time-dependent fluctuations of the normal loading, *J. Geophys. Res.*, 2000, in press.
- Ranjith, K., and J. Rice, Slip dynamics at a dissimilar interface, *J. Mech. Phys. Solids*, 2000, in press.
- Rice, J., and A. Ruina, Stability of steady frictional slipping, *J. Appl. Mech.*, 105, 343–349, 1983.
- Roy, M., and C. Marone, Earthquake nucleation on model faults with rate and state dependent friction: the effects of inertia, *J. Geophys. Res.*, 101, 13,919–13,932, 1996.
- Sato, T., and H. Kanamori, Beginning of earthquakes modeled with the Griffith's fracture criterion, *Bull. Seism. Soc. Am.*, 89, 80–93, 1999.
- Scholz, C., Earthquakes and friction laws, *Nature*, 391, 37–42, 1998.
- Scott, J., T. Masters, and F. Vernon, Three-dimensional velocity structure of the San Jacinto fault zone near Anza, California, I, P-waves, *Geophys. J. Int.*, 119, 611–626, 1994.
- Shaw, B., and J. Rice, Existence of continuum complexity in the elastodynamics of repeated fault ruptures, *J. Geophys. Res.*, 2000, in press.
- Shibazaki, B., and M. Matsu'ura, Transition process from nucleation to high-speed rupture propagation: scaling from stick-slip experiments to natural earthquakes, *Geophys. J. Int.*, 132, 14–30, 1998.
- Sieh, K., et al., Near-field investigations of the Landers earthquake sequence, April to July 1992, *Science*, 260, 171–176, 1993.
- Thurber, C., S. Roecker, W. Ellsworth, Y. Chen, W. Lutter, and R. Sessions, Two-dimensional seismic image of the San Andreas fault in the northern Gabilan Range, central California: Evidence for fluids in the fault zone, *Geophys. Res. Lett.*, 24, 1591–1594, 1997.
- Voisin, C., I. Ionescu, M. Campillo, R. Hassani, and Q. Nguyen, Spectral analysis of the initiation process on a bounded fault zone, *Geophys. J. Int.*, 2000, in press.
- Vrettos, C., Dispersive SH-surface waves in soil deposits of variable shear modulus, *Soil Dynamics and Earthq. Eng.*, 9, 255–264, 1990.
- Wallace, R., and H. Morris, Characteristics of faults and shear zones in deep mines, *Pure Appl. Geophys.*, 124, 107–125, 1986.
- Yamashita, T., and E. Fukuyama, Apparent critical slip displacement caused by the existence of a fault zone, *Geophys. J. Int.*, 125, 459–472, 1996.
- Yamashita, T., and M. Ohnaka, Nucleation process of unstable rupture in the brittle regime: a theoretical approach based on experimental inferred relations, *J. Geophys. Res.*, 96, 17,681–17,690, 1991.

J.-P. Ampuero and J.P. Vilotte, Département de Sismologie (UMR 7580) et Département de Modélisation Physique et Numérique, Institut de Physique du Globe de Paris, 4 Place Jussieu, 75252-Paris, France
 F.J. Sánchez-Sesma, Instituto de Ingeniería, UNAM, Ciudad Universitaria, Apdo. 70-412, Coyoacán, México D.F., México

(Received _____)